https://doi.org/10.5194/egusphere-2024-596
Preprint. Discussion started: 2 April 2024

Using observed urban NO_x sinks to constrain VOC reactivity and the ozone and radical budget in the Seoul Metropolitan Area

Benjamin A. Nault[1,2,*], Katherine R. Travis[3], James H. Crawford[3], Donald R. Blake[4], Pedro Campuzano-Jost[5], Ronald C. Cohen[6], Joshua P. DiGangi[3], Glenn S. Diskin[3], Samuel R. Hall[7], L. Gregory Huey[8], Jose L. Jimenez[5], Kyung-Eun Kim[9], Young Ro Lee[8,a], Isobel J. Simpson[4], Kirk Ullmann[7], Armin Wisthaler[10,11]

[1]CACC, Aerodyne Research, Inc., Billerica, MA, USA
[2]Department of Environmental Health and Engineering, Johns Hopkins University, Baltimore, MD, USA
[3]NASA Langley Research Center, Hampton, VA, USA
[4]Department of Chemistry, University of California, Irvine, CA, USA
[5]CIRES and Department of Chemistry, University of Colorado, Boulder, CO, USA
[6]Department of Chemistry, University of California, Berkeley, CA, USA
[7]Atmospheric Chemistry Observations & Modeling Laboratory, NCAR, Boulder, CO, USA
[8]School of Earth & Atmospheric Sciences, Georgia Institute of Technology, Atlanta, GA, USA
[9]School of Environmental Sciences and Environmental Engineering, Gwangju Institute of Science and Technology, Gwangju, South Korea
[10]University of Oslo, Oslo, Norway
[11]University of Innsbruck, Innsbruck, Austria

[a]Now at Division of Geological and Planetary Sciences, California Institute of Technology, Pasadena, CA, USA

[*]Corresponding author:
Email: bnault@aerodyne.com, bnault1@jh.edu

https://doi.org/10.5194/egusphere-2024-596
Preprint. Discussion started: 2 April 2024

Abstract

Ozone (O_3) is an important secondary pollutant that impacts air quality and human health. Eastern Asia has high regional O_3 background due to the numerous sources and increasing and rapid industrial growth, which impacts the Seoul Metropolitan Area (SMA). However, SMA has also been experiencing increasing O_3 driven by decreasing NO_x emissions, highlighting the role of local, in-situ O_3 production on SMA. Here, comprehensive gas-phase measurements collected on the NASA DC-8 during the NIER/NASA Korea United States-Air Quality (KORUS-AQ) study are used to constrain the instantaneous O_3 production rate over the SMA. The observed NO_x oxidized products support the importance of non-measured peroxy nitrates (PNs) in the O_3 chemistry in SMA, as they accounted for ~49% of the total PNs. Using the total measured PNs (ΣPNs) and alkyl and multifunctional nitrates (ΣANs), unmeasured volatile organic compound (VOC) reactivity (R(VOC)) is constrained and found to range from 1.4 – 2.1 s^{-1}. Combining the observationally constrained R(VOC) with the other measurements on the DC-8, the instantaneous net O_3 production rate, which is as high as ~10 ppbv hr^{-1}, along with the important sinks of O_3 and radical chemistry, are constrained. This analysis shows that ΣPNs play an important role in both the sinks of O_3 and radical chemistry. Since ΣPNs are assumed to be in steady-state, the results here highlight the role ΣPNs play in urban environments in reducing net O_3 production, but ΣPNs can potentially lead to increased net O_3 production downwind due to their short lifetime (~1 hr). The results provide guidance for future measurements to identify the missing R(VOCs) and ΣPNs production.

https://doi.org/10.5194/egusphere-2024-596
Preprint. Discussion started: 2 April 2024

Short Summary

Ozone (O_3) is a pollutant formed from the reactions of gases emitted from various sources. In urban areas, the density of human activities can increase the O_3 formation rate ($P(O_3)$); thus, impact air quality and health. Observations collected over Seoul, South Korea, are used to constrain $P(O_3)$. A high local $P(O_3)$ was found; however, local $P(O_3)$ was partly reduced due to compounds typically ignored. These observations also provide constraints for unmeasured compounds that will impact $P(O_3)$.

https://doi.org/10.5194/egusphere-2024-596
Preprint. Discussion started: 2 April 2024

1. Introduction

Representing global and urban tropospheric ozone (O_3) in chemical transport models (CTMs) is still challenging due to uncertainty in physical and chemical processes that control the O_3 budget (Archibald et al., 2020). One area of uncertainty is underestimated urban volatile organic compounds (VOCs) emissions (von Schneidemesser et al., 2023), which arise form a large number of sources, including some that are very hard to quantify (e.g., cooking and chemical product) (e.g., McDonald et al., 2018; Simpson et al., 2020). Intensive research is also ongoing as to why O_3 is increasing in recent years in urban areas, even with reductions in combustion emissions (e.g., Lyu et al., 2017; Colombi et al., 2023). This O_3 impacts the large populations in urban areas with harmful health effects, including premature mortality (e.g., Cohen et al., 2017).

Tropospheric O_3 production is driven by the catalytic cycling of nitrogen oxides (NO_x = NO + NO_2) fueled by the photoxidation of VOCs, both of which can come from anthropogenic emissions. The chemistry producing O_3 is described in R1 – R6 in Table 1. During daylight hours, VOCs are oxidized by OH (or undergo photolysis) to form an organic peroxy radical ($RO_2^{\cdot}$) in R1a (R1b). If the $RO_2^{\cdot}$ then proceeds through R2a, at least two O_3 molecules are produced. The first O_3 molecule is formed by the photolysis of NO_2 and the reaction of $O(^3P)$ with oxygen (R3 – R4). The second O_3 molecule is formed through the reaction of the alkoxy radical ($RO^{\cdot}$) with oxygen to form the hydroperoxyl radical (HO_2) (R5), which goes on to react with NO to produce NO_2 (R6) and the subsequent reactions described above (R3 – R4). However, some fraction of the time, depending on the number of carbons and functional group (e.g., Espada and Shepson, 2005; Perring et al., 2013; Yeh and Ziemann, 2014), alkyl or multifunctional nitrates (ANs ≡ $RONO_2$) are formed (R2b). The fraction of reactions to form ANs is described by the branching ratio, α. Reaction R2b has been shown to impact O_3 production, depending on the types of VOC emitted,

https://doi.org/10.5194/egusphere-2024-596
Preprint. Discussion started: 2 April 2024

by reducing the fraction of NO_2 that photolyzes to form O_3 in source regions (R3 – R4) (Farmer et al., 2011). As α is a function of the individual VOC's carbon backbone and functional group (e.g., Perring et al., 2013), any uncertainty related to primary VOC emissions and secondary chemistry will directly impact the ability to describe urban O_3 production.

One important subclass of VOCs aldehydes (RCHO), which can either be directly emitted or produced via photooxidation of VOCs (Mellouki et al., 2015; de Gouw et al., 2018; Yuan et al., 2012; Wang et al., 2022). The photooxidation of the aldehyde (R7) in the presence of NO_x can either form acyl peroxy nitrates (R8, PNs = $R(O)O_2NO_2$) or an organic peroxy radical ($RO_2^{\cdot}$) (R9). The competition between R8 to form PNs versus R9 to form $RO_2^{\cdot}$ depends on the NO-to-NO_2 ratio (Nihill et al., 2021). Further, R8 is in thermodynamic equilibrium due to the weak bond strength between the acyl peroxy radical ($R(O)O_2^{\cdot}$) and NO_2. Thus, formation of PNs pose only a temporary loss of NO_2. Finally, it has been observed that aldehydes with longer carbon backbones (e.g., C8s and C9s) from various anthropogenic activities, such as cooking (Coggon et al., 2024; Rao et al., 2010), may have mixing ratios as high as aldehydes typically quantified in field experiments (acetaldehyde and propaldehyde). However, there is larger uncertainty associated with these higher aldehydes in their fate to produce both PNs and ANs (e.g., Hurst Bowman et al., 2003). Missing both these emissions and subsequent chemistry would impact estimates of urban O_3 chemistry.

The fraction of $RO_2^{\cdot}$ forming ANs in R2b and the fraction of $R(O)O_2^{\cdot}$ forming PNs in R8 alter the instantaneous O_3 production ($P(O_3)$) by removing NO_2 and/or the radical species. This is further shown in Figure S1, where an analytical equation to describe R1 – R6 (Farmer et al., 2011), is used to explore how changes in the VOC reactivity (R(VOC)), radical production ($P(HO_x)$), and ANs production and branching ratio, α (R2b), impact the instantaneous $P(O_3)$ (see Sect. S1 for the analytical equation and description). Any changes in $P(HO_x)$, R(VOC), and/or α will impact both

https://doi.org/10.5194/egusphere-2024-596
Preprint. Discussion started: 2 April 2024

the instantaneous $P(O_3)$ as well as the NO_x mixing ratio corresponding to the maximum $P(O_3)$. As these parameters are generally interconnected, investigating all three is important to understand the sources and control of instantaneous $P(O_3)$. Further, R7 – R9 are not included in this traditional description of the analytical equation, as it is assumed PNs are in steady-state (Farmer et al., 2011). Thus, if PNs are not in steady-state, their role in altering $P(O_3)$ may be underestimated.

Increasing surface O_3 is a concern throughout East Asia, including South Korea (Colombi et al., 2023; Gaudel et al., 2018; Kim et al., 2021; Yeo and Kim, 2021). The emissions associated with industry and other anthropogenic activities and the associated photochemistry have impacted regional air quality, leading to high O_3 backgrounds that can impact a country's ability to achieve reduced O_3 exposure for new air quality standards (e.g., Colombi et al., 2023). However, local emissions and photochemistry still play an important role. For example, during the Korea-United States Air Quality (KORUS-AQ) campaign, it was observed between morning and afternoon in the Seoul Metropolitan Area (SMA), O_3 increased by ~20 parts per billion by volume (ppbv) over a background concentration of over 75 ppbv (Crawford et al., 2021). Thus, an understanding of the variables highlighted in Figure S1 are necessary to control both local and regional $P(O_3)$.

One tool typically used to understand the role of regional O_3 and transported O_3 on local O_3 and impacts of local emission controls on O_3 are CTMs. As shown in Park et al. (2021), for the SMA, CTMs typically underestimate the observed O_3 and formaldehyde. While the low O_3 could be partially related to underestimated transport (e.g., Seo et al., 2018) or resolution of the CTM (e.g., Jo et al., 2023; Park et al., 2021), the low bias also observed for modeled formaldehyde indicates overall (a) too little VOCs and thus too low R(VOC) (Brune et al., 2022; H. Kim et al., 2022), (b) missing photochemical products from missing VOCs, including oxygenated VOCs (OVOCs) that contribute to $P(HO_x)$ (Brune et al., 2022; H. Kim et al., 2022; Lee et al., 2022; Wang

https://doi.org/10.5194/egusphere-2024-596
Preprint. Discussion started: 2 April 2024

et al., 2022), and (c) likely missing PNs and ANs from the underestimated VOCs related to the underestimated R(VOC) (Lee et al., 2022; Park et al., 2021). Missing (a) – (c) will bias the instantaneous $P(O_3)$ (Figure S1), impacting the ability to investigate what policies should be implemented to reduce O_3.

To better understand what controls the instantaneous $P(O_3)$ over SMA, observations collected on the NASA DC-8 during KORUS-AQ are used to constrain the three variables highlighted in Figure S1—R(VOC), HO_x production and loss, and ANs and PNs production. Observational constraints on these three parameters provide a means to investigate the instantaneous $P(O_3)$ over SMA and the major classes of contributors to O_3 and HO_x production and loss. These results are discussed and placed into the context of improving our knowledge about O_3 production in an urban environment.

2. Methods and Data Description

2.1 KORUS-AQ and DC-8 Descriptions

The KORUS-AQ campaign was a multi-national project that was conducted in May – June, 2016, led by South Korea's National Institute of Environmental Research (NIER) and United States National Aeronautics and Space Administration (NASA). The project was conducted in South Korea and the surrounding seas with numerous airborne platforms, research vessels, and ground sites (Crawford et al., 2021). The study here focuses on the observations collected on the NASA DC-8.

The instrument payload, flights, and observations have been described in other studies (Crawford et al., 2021; Schroeder et al., 2020; Brune et al., 2022; Lee et al., 2022). Briefly, the DC-8 was stationed at Osan Air Force Base, Pyeongtaek, South Korea, which is approximately 60

https://doi.org/10.5194/egusphere-2024-596
Preprint. Discussion started: 2 April 2024

km south of Seoul. A total of 20 research flights were conducted with the DC-8. Part of each research flights included a stereo-route in the SMA in the morning (~09:00 local time), midday (~12:00 local time), and afternoon (~15:00 local time), which included a missed approach over Seoul Air Base (< 15 km from Seoul city center) and a fly-over of the Olympic Park and Taehwa Forest Research sites (Figure 1). A total of 55 descents over Olympic Park and 53 spirals over Taehwa Forest Research site were conducted (Crawford et al., 2021). Only observations from the DC-8 after 11:00 local time are used here to ensure that the boundary layer has grown and stabilized and to minimize any influence from residual layer mixing into the boundary layer and/or titration of O_3 by NO (R10). We analyze data collected below 2 km and between 127.10 – 127.67°E and 37.22 – 37.69°N to focus on the boundary layer in the SMA without influence from industrial emissions along the western South Korean coast (Crawford et al., 2021).

During KORUS-AQ, four different meteorological periods, as described by Peterson et al. (2019), impacted the region. These periods included a Dynamic period from 1 – 16 May, where there were a series of frontal passages; a Stagnant period from 17 – 22 May, where it was dry, clear, and stagnant; Transport/Haze period from 25 – 31 May, where long-range transport and hazy conditions with high humidity and cloud cover prevailed; and, a Blocking period from 1 – 7 June, where blocking conditions minimized transport (Peterson et al., 2019). However, as discussed in Sect. 3.2, conditions did not impact the general trends and chemistry and thus the whole campaign has been analyzed together.

The observations used for the analysis are shown in Table 2, along with the associated references. The 1-min merged data from the DC-8 is used here (KORUS-AQ Science Team, 2023). For data missing due to frequency of measurements (e.g., VOCs from WAS), data was filled in a similar approach as Schroeder et al. (2020), in that VOCs with missing data were filled by the

https://doi.org/10.5194/egusphere-2024-596
Preprint. Discussion started: 2 April 2024

linear relationship of that VOC with VOCs measured more frequently. This step was necessary for the observations used in the diel steady-state calculations described in Sect. 2.2. Note, the TD-LIF NO_2 (see Table 2) was used throughout this study and discussed in Sect. S2 and Figure S2 – S3 as it generally agreed better with steady-state calculated NO_2-to-NO ratios than the chemiluminescence NO_2.

2.2 F0AM Box Model Diel Steady-State Calculations for Missing Reactivity and Peroxynitrate Budget Analysis

We use the F0AM box model (Wolfe et al., 2016) with chemistry from the MCMv3.3.1 (Jenkin et al., 2015) to simulate production of PNs and formaldehyde using 1-min merged data, as described in Sect. 2.1. As in Schroeder et al. (2020), we simulate each aircraft observation in diurnal cycle mode until the diurnal cycle for each species reaches convergence within 1%. We constrain concentrations of NO, O_3, H_2O_2, HNO_3, CO, CH_4, H_2, and all measured or estimated VOCs given in Table 2 and Table S1. We allow the model to freely calculate NO_2, formaldehyde, and all PNs, including PAN and PPN, for when calculating the budget of PNs. However, for the acyl peroxy radical mixing ratios to calculate O_x and HO_x budget (Sect. 2.3), PAN and PPN were constrained by observations. We use a dilution constant of 12 hours, according to Brune et al. (2022). Model evaluation is discussed in Sect. 3.4. The contribution of individual VOCs to PAN was calculated by reducing precursor VOCs by 20% and multiplying the resulting impact on the peroxy acetyl radical ($CH_3C(O)O_2^{\cdot}$) by 5. Other acyl peroxy nitrates (higher PNs) are lumped into categories based on their primary precursor species from Table S2, species currently typically

https://doi.org/10.5194/egusphere-2024-596
Preprint. Discussion started: 2 April 2024

193 measured (e.g., PPN) or contributes a large fraction of the total higher PNs budget (greater than
194 >2%; e.g., PHAN and MPAN).
195
196 **2.3 Calculation of Instantaneous Ozone and HO_x Production and Loss**
197 An experimental budget for the production and loss of O_x ($O_x = O_3 + NO_2$) and HO_x (HO_x
198 $= OH + HO_2 + RO_2^{\cdot} + R(O)O_2^{\cdot}$) is described here. NO_2 and O_3 are combined to reduce any potential
199 impact from titration via O_3 reaction with NO (R10). The budget analysis includes field-measured
200 quantities (mixing ratios and photolysis rates, Table 2), results from F0AM (Sect. 2.2), estimated
201 missing R(VOC) (Sect. 3.2) and published kinetic rate constants (see Table 1 for references). The
202 rate of production or destruction is calculated with the following equations (Eq. 1 – 7) below. Note,
203 these equations differ from Schroeder et al. (2020) in that (a) ANs and PNs chemistry are explicitly
204 included and (b) the reaction of O_3 with alkenes is excluded as this reaction contributed a minor
205 loss to O_3 (< 1%).

206 $$P_{O_x} = \sum_i (1-\alpha_{eff}) k_{RO_{2,i}+NO} [RO_{2,i}^{\cdot}][NO] + k_{HO_2+NO}[HO_2][NO] \quad (1)$$

207 $$L_{O_x} = k_{NO_2+OH}[NO_2][OH] + k_{O_3+OH}[O_3][OH] + f \times j_{O^1D}[O_3] +$$

208 $$k_{HO_2+O_3}[HO_2][O_3] + net(PNs) \quad (2)$$

209 $$net(PNs) = \beta k_{R(O)O_2^{\cdot}+NO_2}[R(O)O_2^{\cdot}][NO_2] - (1-\beta) k_{decomposition}[PNs] \quad (3)$$

210 $$\beta = \frac{k_{RC(O)O_2+NO_2}[NO_2]}{k_{RC(O)O_2+NO_2}[NO_2] + k_{RC(O)O_2+NO}[NO]} \quad (4)$$

211 $$P(HO_x) = 2f \times j_{O^1D}[O_3] + 2j_{H_2O_2}[H_2O_2] + 2j_{CH_2O \rightarrow H+HCO}[CH_2O] + 2j_{CHOCHO}[CHOCHO] +$$

212 $$2j_{CH_3OOH}[CH_3OOH] + 2j_{CH_3CHO}[CH_3CHO] + 2j_{CH_3C(O)CH_3}[CH_3C(O)CH_3] +$$

213 $$2j_{CH_3CH_2C(O)CH_3}[CH_3CH_2C(O)CH_2] \quad (5)$$

https://doi.org/10.5194/egusphere-2024-596
Preprint. Discussion started: 2 April 2024

$$L(HO_x) = k_{NO_2+OH}[NO_2][OH] + \sum_i \alpha_{eff} k_{RO_{2,i}+NO}[RO_{2,i}^{\cdot}][NO] + 2k_{HO_2+HO_2}[HO_2][HO_2] + 2k_{RO_2+RO_2}[RO_2^{\cdot}][RO_2^{\cdot}] + 2k_{HO_2+RO_2}[HO_2][RO_2^{\cdot}] + net(PNs) \quad (6)$$

$$[RO_2^{\cdot}] = \frac{\sum_i k_{OH+VOC,i}[VOC_i][OH]}{(1-\alpha_{eff})k_{RO_2+NO}[NO] + k_{RO_2+HO_2}[HO_2]} \quad (7)$$

Here, k is the rate constant for compound, i, with the associated compound listed, α_{eff} is the effective branching ratio for R2a and R2b for the observations (Sect. 3.2), f is the fraction that O^1D that reacts with water to form OH versus reacting with a third body molecule to form O^3P, β is the fraction the $R(O)O_2^{\cdot}$ that reacts with NO_2 versus NO, and j is the measured photolysis frequency (Table 2). Note, $R(O)O_2^{\cdot}$ is not included in Eq. 7 as (a) it is assumed the initial production of $R(O)O_2^{\cdot}$ is captured with the reaction of OH with VOC and (b) $R(O)O_2^{\cdot}$ accounts for a small fraction of the total RO_2 (< 10%). Not including $R(O)O_2^{\cdot}$ in Eq. 7 may lead to a small underestimation of total $RO_2^{\cdot}$. Finally, HO_2 calculated from F0AM is used in the equations to determine the O_x and HO_x budget.

3. Observational constraints on NO_x organic oxidation chemistry

In the Sect. 3.1, the detailed observations from the DC-8 during KORUS-AQ provided measurements that allow us to test our understanding of NO_x oxidation into total NO_z (NO_z = higher NO_x oxides, including ΣPNs, ΣANs, HNO_3 and particulate nitrate, pNO_3), which is needed for the remainder of the analysis. Sect. 3.2 to 3.4 will focus on the organic NO_z chemistry. This is due to the chemistry and dynamics impacting the total inorganic nitrate chemistry that has been discussed recently (Travis et al., 2022; Jordan et al., 2020).

3.1 NO_x and its oxidation products

https://doi.org/10.5194/egusphere-2024-596
Preprint. Discussion started: 2 April 2024

The average NO_x mixing ratios observed by the NASA DC-8 in the SMA below 2 km after 11:00 local time is shown in Figure 1. As NO_x is mainly emitted from anthropogenic activities, such as combustion emissions, in an urban environment, the largest NO_x mixing ratios are observed between Olympic Park and the missed approach, as this area included downtown SMA. As the DC-8 flies from the missed approach toward Taehwa Research Site, the NO_x mixing ratios decreases. The combination of reduced emissions, chemical reactions, and dilution and mixing reduces the NO_x mixing ratios away from the city. An understanding of these processes is important for urban $P(O_x)$.

On the DC-8, there were multiple measurements of various speciated and total family contribution towards NO_z (Table 2). The comparison of the speciated and measured NO_z is investigated in Figure 2 for observations over SMA. When only speciated PNs (GT) and ANs (CIT + WAS) and gas-phase nitrate (HNO_3) are compared to the NO_z (NO_y (NCAR) – (NO (NCAR) + NO_2 (TD-LIF)), only 46% of the NO_z can be explained. This is not completely unexpected, as multiple studies have indicated that the speciated ANs measurements are typically lower than the total ANs measurements (Perring et al., 2010; Fisher et al., 2016). Further, pNO_3 has been found to be important for total nitrate budget in the SMA (e.g., Travis et al., 2022). Chemiluminescence measurements of gas-phase NO_y have been found to efficiently measure pNO_3, depending on the sensitivity to pNO_3 enhancements or exclusions (Bourgeois et al., 2022); thus, it is expected that missing ANs and pNO_3 are necessary to close the NO_z budget. Adding the measured pNO_3 to the speciated PNs (GT) and ANs (CIT + WAS) and gas-phase nitric acid, 81% of NO_z can be explained. This barely overlaps the combined uncertainty of the measurements (~26%). Total PNs and ANs, measured by TD-LIF, are needed to close of the total NO_z budget.

https://doi.org/10.5194/egusphere-2024-596
Preprint. Discussion started: 2 April 2024

The breakdown of the NO_z budget over the SMA as the airmasses photochemically ages (decreasing NO_x contribution to total NO_y) is shown in Figure 2b. During KORUS-AQ, ~56% of NO_z was inorganic (gas- and particle-phase nitrate), ranging from 52% to 62%; the remaining NO_z was organic (PNs and ANs). Approximately 74% of the total ANs were not speciated (range 73% to 76%). Speciated PNs species, such as PAN (peroxy acetyl nitrate), account for a mean 51% of the total PNs (range 47 to 59%), much lower than typically observed in prior studies (e.g., Wooldridge et al., 2010). In these prior studies, the speciated PN species (typically PAN + PPN (peroxy propionyl nitrate)) accounted for 90 – 100% of the ΣPNs, except for some select cases attributed to poor inlet design (Wooldridge et al., 2010). PAN accounted for the majority of the speciated PNs, with the remaining speciated PNs (PPN + PBzN (peroxy benzoyl nitrate) + APAN (peroxy acryloyl nitrate)) accounting for ~1%. However, during KORUS-AQ, Lee et al. (2022) observed that PAN contributed only 60% of calculated total PNs in industrial plumes near the SMA. Thus, the VOC emissions in and near SMA potentially lead to PNs typically not directly measured; this is explored more in Sect. 3.4

As NO_x decreases from ~30 ppbv to 4 ppbv, the contribution of organic NO_z increases (Figure 2b). At about 4 ppbv, the contribution of organic NO_z starts to decrease. Further, the contribution of the different organic NO_z species changes. For example, from ~30 ppbv to 4 ppbv, the un-speciated ΣPNs contributes the majority of the organic NO_z budget (~39%). Below ~4 ppbv, the contribution of un-speciated ΣPNs decreases and the PAN contribution increases. The change in contribution of PNs is due to changes in the PN precursors (e.g., combination short-lived precursors oxidizing to $CH_3C(O)O_2^{\cdot}$ and thermal decomposition of the higher PNs (higher PNs = ΣPNs – PAN)). On the other hand, the contribution of un-speciated ΣANs remains relatively constant with NO_x (~6% of total NO_z). However, the type of ANs is most likely changing with

https://doi.org/10.5194/egusphere-2024-596
Preprint. Discussion started: 2 April 2024

NO_x due to the lifetime of the ANs precursors and/or the lifetime of ANs. Less is known about the lifetime of ANs derived from anthropogenically emitted VOCs compared to those from biogenic VOCs (González-Sánchez et al., 2023; Picquet-Varrault et al., 2020; Zare et al., 2018). On average unknown ANs and PNs account for ~24% of the observed NO_z on average.

3.2 Meteorological impact on NO_x oxidation

As discussed in Sect. 2.1 and various prior studies, four different meteorological conditions impacted the observations during KORUS-AQ (Peterson et al., 2019). The impact of the meteorological conditions on NO_x oxidation was investigated by plotting two metrics of NO_x oxidation—O_x versus ΣANs and ΣPNs versus formaldehyde (Figure 3). The implications of both plots are further discussed in Sect. 3.3 and 3.4, respectively. Briefly, O_x versus ΣANs and ΣPNs versus formaldehyde are competitive products from the reaction of $RO_2^{\cdot}$ or $R(O)O_2^{\cdot}$ with NO_x (R2a versus R2b or R8 versus R9). The different meteorological periods corresponded to differences in temperatures and amount of photolysis due to cloud cover (Peterson et al., 2019). Thus, these different periods may impact gas-phase chemistry and/or VOC emissions. However, as demonstrated in Figure 3, there are minimal systematic differences in the trends observed for the two NO_x oxidation products as there is no systematic shift in the trends or scatter observed in Figure 3. This suggests that the data does not have to be separated by meteorological conditions.

3.3 Production of ANs to constrain R(VOC)

Observations of un-speciated ANs and PNs imply missing VOCs that impact O_3 chemistry. The relationship of ANs to O_x can provide a method to investigate this source. This relationship provides an estimate of the effective branching ratio, α, for the observed VOC mix (Perring et al.,

https://doi.org/10.5194/egusphere-2024-596
Preprint. Discussion started: 2 April 2024

2013 and references therein). The value of this relationship stems from the reactions discussed above (R1 – R6) in that upon the oxidation of VOCs, some fraction of the time, $RO_2^{\cdot}$ reacts with NO to form an AN molecule and the remainder of the time the reaction goes to form O_3. This is expressed with the following equations:

$$P_{\Sigma ANs} = \sum \alpha_i \, k_{OH+VOCi}[\mathrm{OH}][\mathrm{VOC_i}] \quad (8)$$

$$P(\mathrm{O_x}) = \sum_i \gamma_i (1-\alpha_i) \, k_{OH+VOC_i}[\mathrm{OH}][\mathrm{VOC}_i] \quad (9)$$

Here, α is the effective branching ratio in the reaction of $RO_2^{\cdot}$ with NO to form ANs versus $RO^{\cdot}$ (R2), k is the OH rate constant with VOC, i, and γ is the number of O_3 molecules formed per oxidation of VOC, i. The γ, calculated for the observed and calculated compounds from F0AM using the values from MCM (Jenkin et al., 2015), is found to be, on average, 1.53, which is lower than the value of 2 typically assumed in prior studies (e.g., Perring et al., 2013). This lower γ is due to the role of CO and CH_2O to the total reactivity. After the boundary layer height has stabilized (e.g., after 11:00 am LT used here) and is near enough (e.g., less than 1 day aging) to the VOC source to ignore deposition and entrainment, Eq. 8 and 9 can be combined to approximate the change in O_x per molecule ΣAN formed:

$$\frac{\Delta O_x}{\Delta \Sigma ANs} \approx \frac{P_{O_x}}{P\Sigma ANs} \approx \frac{1.53(1-\alpha)}{\alpha} \quad (10)$$

For this equation to be valid, α needs to be relatively small (α << 1), which is true for VOCs, as maximum α for the conditions of KORUS-AQ is expected to be 0.35 (Orlando and Tyndall, 2012; Perring et al., 2013; Yeh and Ziemann, 2014). Note, though Eq. 10 can be used at short photochemical ages due to minimal impact from physical loss processes, chemical loss processes may impact the assumptions in Eq. 10 and are discussed in more detail below.

Over the SMA during KORUS-AQ, the slope between O_x and ΣANs was observed to be 40.5±1.8 (Figure 3a), with an R^2 = 0.60. Using Eq. 10, this translates to an effective branching

https://doi.org/10.5194/egusphere-2024-596
Preprint. Discussion started: 2 April 2024

ratio (α_{eff}), of 0.036. For other urban locations around the world, this slope has ranged from 13 – 47 (Farmer et al., 2011; Kenagy et al., 2020; Perring et al., 2010; Rosen et al., 2004), leading to an effective α between 0.04 and 0.15, assuming a γ of 2 instead of the calculated γ used here. Thus, the α_{eff} observed over SMA during KORUS-AQ is similar to other urban locations (Houston = 0.05 (Rosen et al., 2004) and South Korea = 0.05 (Kenagy et al., 2021)) but much lower than observed for Mexico City = 0.07 – 0.12 (Perring et al., 2010; Farmer et al., 2011) and Denver = 0.16 (Kenagy et al., 2020). This suggests that VOCs with low α dominate the total R(VOC) and production of ANs in SMA. The VOCs in SMA that dominate R(VOCs), including OVOCs, alkenes, and aromatics (Schroeder et al., 2020; Simpson et al., 2020), generally have lower α (Perring et al., 2013 and references therein; Orlando and Tyndall, 2012).

We use the observed VOCs (Table 2) to calculate α_{eff} from this mixture to compare to the calculated α_{eff} of 0.036 derived from the slope of O_x versus ΣANs in Figure 3a, as shown in Figure 4. The R(VOC) calculated from the observed VOCs and from the intermediates produced by the F0AM model, described in Sect. 2.2, are shown in Figure 4a, and the reactivity weighted α for the observations is shown in Figure 4b. As has been observed in other urban environments (e.g., Hansen et al., 2021; Whalley et al., 2016; Whalley et al., 2021; Yang et al., 2022;), measured OVOCs contribute the most to the calculated R(VOC) for all NO_x mixing ratios (32 – 48%). The unmeasured OVOCs (F0AM species) contributed 17 – 28% of the calculated reactivity. The F0AM species reactivity ranged from 0.45 – 1.78 s^{-1}, which is a similar increase in total OH reactivity observed by Brune et al. (2022) over South Korea. At higher NO_x mixing ratios, primary, more reactive VOCs (e.g., alkanes, alkenes, aromatics) contribute an important fraction (> 25%) of the R(VOC). As there are interferences in the total OH reactivity measurement at high NO_x (Brune et al., 2022), we are unable to determine the extent to which the observed and modeled reactivity

https://doi.org/10.5194/egusphere-2024-596
Preprint. Discussion started: 2 April 2024

captures total OH reactivity in the SMA above a NO_x value of approximately 4 ppbv. At lower NO_x mixing ratios, ~33% of the R(VOC) is missing (calculated R(VOC), including F0AM species, ~3.0 s^{-1} and measured R(VOC) from Penn State—see Table 2—is 4.5 s^{-1}).

Numerous other urban studies have observed unmeasured OH reactivity, which is assumed to be unmeasured R(VOC), as the inorganic OH reactivity is typically well covered by measurements. This unmeasured R(VOC) has ranged from ~3 s^{-1} to ~10 s^{-1} (e.g., Brune et al., 2022; Hansen et al., 2021; Kim et al., 2016; Ma et al., 2022; Tan et al., 2019; Whalley et al., 2016; Whalley et al., 2021). Over the SMA, the difference between measured and calculated R(VOC) was ~1.5 s^{-1} at low NO_x and unknown at high NO_x mixing ratios. The lower difference may be related to the comparison occurring for observations at low NO_x, when the very reactive material has either reacted into compounds measured on the DC-8 (e.g., formaldehyde, acetaldehyde, etc.), diluted to low enough concentrations to be negligible for R(VOC), or undergone deposition or partitioning to the particle-phase.

At higher NO_x mixing ratios, which is more representative of fresh emissions, these more reactive compounds typically not measured are expected to lead to a higher difference between the calculated and observed R(VOC). Prior studies with more comprehensive measurements found these more reactive compounds and their secondary products contributed an important fraction towards the R(VOC) (e.g., Whalley et al., 2016). Thus, to determine if these unmeasured VOCs potentially contribute to the R(VOC), and thus $P(O_x)$, in SMA, another means to constrain their contributions is necessary. One potential means to constrain the total R(VOC) is by using the observed ΣANs and O_x and assuming the observations are from the instantaneous production of both species (e.g., the assumption used for Figure 3a).

https://doi.org/10.5194/egusphere-2024-596
Preprint. Discussion started: 2 April 2024

To estimate the unmeasured R(VOC), Eq. 10 is used without cancelling out terms and expanded into the measured and unmeasured R(VOC) and α:

$$\frac{\Delta O_x}{\Delta \sum ANs} = \frac{\gamma RVOC_m[\mathrm{OH}]+\gamma RVOC_u[\mathrm{OH}]-\gamma\alpha_m RVOC_m[\mathrm{OH}]-\gamma\alpha_u RVOC_u[\mathrm{OH}]}{\alpha_m RVOC_m[\mathrm{OH}]+\alpha_u RVOC_u[\mathrm{OH}]} \quad (11)$$

Here, $\frac{\Delta O_x}{\Delta \sum ANs}$ is the slope from Figure 3a, γ is the number of O_3 molecules formed per oxidation of VOC, which is 1.53 for this study, R(VOC) is the VOC reactivity, which is its OH oxidation rate constant and its concentration (k×[VOC]) in units s^{-1}, α is the branching ratio for R2 (Table 1), and *m* and *u* correspond to measured and unmeasured RVOC and α. The rate constants for the measured VOCs are listed in Table 1, the reactivity for F0AM is taken directly from F0AM, and α is either from MCM (Jenkin et al., 2015) or Perring et al. (2013) for observations or assumed to be 0.05 for F0AM secondary products. The equation is rearranged and solved for $RVOC_u$, using different values of α_u (e.g., 0.00 – 0.30, values typical α).

As discussed in Sect. S3 in the Supp. Information, there are numerous assumptions and potential sources of uncertainty in the simplified version of Eq. 11. A thorough analysis and discussion of these assumptions are discussed in Sect. S3. The potentially most important assumption is that chemical loss is negligible in solving Eq. 11. However, due to the expected relatively short lifetime of ∑ANs, the chemical loss of both O_x and ANs nearly cancel each other, leading to similar results in considering or neglecting these loss terms in Eq. 11. Further, as ∑ANs chemical loss has uncertainty, especially for ANs produced from anthropogenic VOC oxidation, the use of Eq. 11 reduces some of these uncertainties in comparison to Eq. S9. Thus, for the remainer of the paper, the values calculated from Eq. 11 will be used.

For the range of missing α assumed, an α = 0.10 for the unmeasured R(VOC) provides the best agreement with the observed R(VOC) ("From PSU" is the Penn State OH Reactivity with inorganic reactivity subtracted out) for all observations where NO_x < 4 ppbv. Further, it is found

https://doi.org/10.5194/egusphere-2024-596
Preprint. Discussion started: 2 April 2024

that α ranging from 0.075 – 0.125 encompasses the associated uncertainty with the observed R(VOC) (±0.64 s^{-1} (Brune et al., 2019)). This leads to an average unmeasured R(VOC) of $1.7^{+1.1}_{-0.4}$.

The associated total missing R(VOC) for the assumed α of 0.10 ranges from 1.4 to 2.1 s^{-1}. Assuming typical rate constants for emitted VOCs, assuming it is comparable to semi- and intermediate-VOCs, and their associated secondary products (~1 – 4×10^{-11} cm^3 $molec.^{-1}$ s^{-1} (Ma et al., 2017; Zhao et al., 2014)), the total missing reactivity would be equivalent to ~1 – 8 ppbv. Zhao et al. (2014) observed ~12 μg m^{-3} of semi- and intermediate-VOCs near Los Angeles, CA, during the CalNex study. Depending on the molecular weight assumed, this translates to ~1 to 2 ppbv. Nault et al. (2018) found that ~5 – 8 ppbv of VOCs were needed to explain the observed secondary organic aerosol production over the SMA, depending on the molecular weight assumed for the VOC. Further, Kenagy et al. (2021) also found that known chemistry could only account for ~33% of the observed ANs and missing sources of lower volatility VOCs to produce anthropogenically-derived ANs were necessary. Finally, Whalley et al. (2016) found that addition of unassigned VOCs and their associated oxidation products led to a reactivity of ~1.6 s^{-1}, leading to ~1 – 6 ppbv missing R(VOC). Thus, the reactivity and equivalent mixing ratios estimated here appear plausible and warrant future measurements to understand this unmeasured reactivity sources.

One important aspect of this unmeasured R(VOC) is that it should not be considered one or a couple of VOCs emitted and contributing 1 – 8 ppbv of VOC in the atmosphere. Instead, it will be the emitted VOCs and its oxidation products summed together to form the 1 – 8 ppbv of unmeasured VOCs in the atmosphere.

One possible missing VOC is nonanal, which is associated with cooking emissions (Rao et al., 2010; Sai et al., 2012; Schauer et al., 2002) and vegetative emissions (Hurst Bowman et al., 2003). Kim et al. (2018) observed cooking organic aerosols at a ground site in SMA, indicating

https://doi.org/10.5194/egusphere-2024-596
Preprint. Discussion started: 2 April 2024

that there should be associated gas-phase emissions from cooking. Nonanal has recently been suggested to be a potential interference compound with isoprene measurements on a PTR-MS (Coggon et al., 2024; Wargocki et al., 2023). Comparisons of isoprene measured by the PTR-MS and WAS during KORUS-AQ (Figure S5) shows at increasing NO_x mixing ratios (closer to emission sources), the difference between the PTR-MS and WAS isoprene mixing ratios increases. This suggests that there are potential unmeasured OVOCs and/or other C_5H_8 alkenes at high NO_x ratios that cannot be easily determined by the difference between the PTR-MS and WAS. Continuing to use nonanal as a surrogate for this unmeasured OVOC, nonanal has a rate constant consistent with the values used above for the missing R(VOC) (3.6×10^{-11} cm^3 $molec.^{-1}$ s^{-1} (Hurst Bowman et al., 2003)). Further, nonanal has an estimated high α of ~0.2 (Hurst Bowman et al., 2003). As typical nonanal mixing ratios have been observed or estimated to be < 500 pptv, this suggests that nonanal or similar OVOCs may contribute to some of the missing reactivity (< 0.45 s^{-1}). Finally, nonanal may be an important higher PNs precursor (see Sect. 3.4 for more discussion about un-speciated higher PNs).

OVOC emissions are generally considered to be an important fraction of R(VOC) for urban emissions (de Gouw et al., 2018; Gkatzelis et al., 2021; McDonald et al., 2018; Ma et al., 2022; Simpson et al., 2020; Wang et al., 2022; Yang et al., 2022). However, the α for OVOC is potentially smaller than alkanes, though it is highly unconstrained (Orlando and Tyndall, 2012). Note, higher OVOCs have been understudied and thus may have higher α (e.g., nonanal). Thus, if the missing reactivity is mainly OVOCs and it is assumed their α is low, compounds with α > 0.15 will be needed for the budget closure shown here. Likely compounds with high α include alkanes, cycloalkenes/alkenes, and aromatics, though the latter is also highly uncertain. Alkanes have typically been a small source for the R(VOC) in urban environments (e.g., McDonald et al., 2018;

https://doi.org/10.5194/egusphere-2024-596
Preprint. Discussion started: 2 April 2024

Simpson et al., 2020; Whalley et al., 2016). Though aromatics contribute a significant fraction of R(VOC) in different Asian urban environments (Brune et al., 2022; Schroeder et al., 2020; Simpson et al., 2020; Whalley et al., 2021), the majority of the aromatic R(VOC) is considered to be measured by WAS over SMA during KORUS-AQ (e.g., measured aromatics account for ~81% of aromatic reactivity in McDonald et al. (2018) and 98% of aromatic reactivity in Whalley et al. (2016), where both studies had more complete VOC measurements). Finally, the cycloalkenes/alkenes originate from numerous anthropogenic sources (e.g., McDonald et al., 2018; Simpson et al., 2020). One subclass of cycloalkenes includes monoterpenes. Similar to the comparison of isoprene between PTR-MS and WAS, the difference in monoterpenes between these two measurements increases with increasing NO_x (Figure S6). As the interfering compound(s) measured by the PTR-MS and whether they are oxygenated or not is not known, only the WAS monoterpenes are used in this analysis of calculating R(VOC). Assuming the limonene rate constant, the difference between the PTR-MS and WAS monoterpenes raises the terpene reactivity by 0.05 – 0.30 s^{-1}. Though this does not include any associated photochemical products from the oxidation of monoterpenes and can improve the closure, it does not explain the total missing reactivity (1.4 – 2.1 s^{-1}). Thus, the missing R(VOC) is most likely a combination of OVOCs and cycloalkenes/alkenes.

3.4 Sources of PNs over SMA

As shown in Figure 2, ΣPNs account for a larger fraction of the total NO_z budget than ΣANs. ΣPNs are known to be a temporary sink of NO_x and radicals ($R(O)O_2^{\cdot}$) due to their short thermal lifetime (~1 hr). Thus, the NO_x emitted in SMA is being transported regionally, impacting the $P(O_x)$.

https://doi.org/10.5194/egusphere-2024-596
Preprint. Discussion started: 2 April 2024

In Figure 3b, ΣPNs shows some correlation with formaldehyde. Both are secondary products from the photooxidation of VOCs and have short lifetimes, leading to the correlation. However, above 4 ppbv formaldehyde, the correlation shifts as ΣPNs increases more rapidly than formaldehyde. As shown in Figure S7, this change in the relationship between ΣPNs versus formaldehyde is due to changes in the competition in the reaction of the acyl peroxy radical ($R(O)O_2^{\cdot}$) between NO_2 and NO. At low NO-to-NO_2 ratios, R8 is more favorable, leading to more efficient production of PNs over formaldehyde. As NO-to-NO_2 ratios increase (NO becomes comparable to NO_2), R9 becomes more dominant, leading to less production of PNs.

To further explore the sources of both PAN and the higher ΣPNs, the F0AM model (Wolfe et al., 2016) was used to predict ΣPNs, constrained by the observed VOCs precursors (Table 2). F0AM shows minimal bias in the predicted formaldehyde, NO_2, and OH (Figure S8). As discussed in Sect. 3.3, though, there is missing R(VOC) of $1.7^{+1.1}_{-0.4}$ s^{-1}. A sensitivity analysis in adding this missing reactivity to F0AM on predicted OH and formaldehyde was conducted (Sect. S4 and Figure S9 – S10). Both OH and formaldehyde are found to be buffered with the addition of this low amount of R(VOC). Thus, though there is good agreement in these intermediate products between observation and F0AM, this analysis for the sources of PAN and higher ΣPNs is expected to be a lower limit. This missing R(VOC) is further observed in the F0AM-predicted higher PNs (ΣPNs-PAN) versus formaldehyde, as a general underestimation in the total higher PNs compared to observations is observed (Figure 5a). PAN was excluded as F0AM overestimated the mixing ratios of PAN by approximately a factor of 2 (Figure S8e). Note, F0AM also overpredicted the PPN mixing ratios, but to a lesser extent than PAN (~50%; Figure S8f). The differences in predicted versus observed PNs may be associated with assumed background, dilution, and/or temperature used to reach steady-state (Schroeder et al., 2020). Thus, the results from F0AM will

https://doi.org/10.5194/egusphere-2024-596
Preprint. Discussion started: 2 April 2024

provide qualitative insight into sources and chemistry that should be investigated to better understand PN chemistry in SMA.

The classes of compounds producing higher PNs in F0AM are shown in Figure 5b. The classes of compounds were selected from the parent VOC which was oxidized into the higher PN (Table S2). Individual PNs with high contributions and/or are typically measured (PPN, PBzN, and MPAN (methacryloyl peroxy nitrate)) or are a large fraction of PNs but have yet to be measured in ambient conditions (PHAN) are shown without any connection to the parent VOC. Further, both PHAN and PPN have numerous precursors while many of the other higher PNs modeled by F0AM are generally associated with one precursor. At high NO_x mixing ratios, the more reactive VOCs (aromatics, terpenes) contribute a large fraction of the higher PNs (>35% for NO_x > 4 ppbv). As the air moves away from SMA (lower NO_x mixing ratios), contributions of higher PNs from longer-lived compounds (e.g., alkanes) and later generation oxidation products start dominating.

An interesting trend is observed for PPN and PHAN. Both peroxy acyl radicals for PPN and PHAN ($C_2H_5C(O)O_2^{\cdot}$ and $CH_2(OH)C(O)O_2^{\cdot}$, respectively) are products from photooxidation of many VOCs, including aromatics, alkanes, and methyl ethyl ketone (MEK). However, the fractional contribution of PPN to higher PNs remains constant with decreasing NO_x while the fractional contribution of PHAN increases with decreasing NO_x (Figure 5b). This stems from the sources of $C_2H_5C(O)O_2^{\cdot}$ versus $CH_2(OH)C(O)O_2^{\cdot}$. The MCM mechanism, which is used for F0AM, produces $C_2H_5C(O)O_2^{\cdot}$ from the photooxidation from both short- and long-lived species (isoprene, C8-aromatics, toluene, ethanol, MEK, propane, and C4-alkanes) while $CH_2(OH)C(O)O_2^{\cdot}$ is produced from the photooxidation of isoprene and ethene. For $CH_2(OH)C(O)O_2^{\cdot}$, the production is through minor channels in the photooxidation of isoprene

https://doi.org/10.5194/egusphere-2024-596
Preprint. Discussion started: 2 April 2024

(~3% yield directly from isoprene and ~20% as a secondary product (Galloway et al., 2011)). Ethene is relatively long-lived, with a lifetime ~7 hrs (OH = 5×10^6 molec. cm^{-3}) leading to the delay in the production of PHAN.

The results here in general indicate more speciated measurements of higher PNs are needed. However, as highlighted in Figure 5, improved detection of or measurements of PBzN, PHAN, and MPAN would allow for furthering our knowledge in PNs chemistry in urban environments and their role in controlling O_x production.

A qualitative investigation of the precursors of PAN predicted by F0AM are shown in Figure 5c. This provides a basis for further investigation of the sources over the SMA region for PAN as (a) F0AM over-predicts PAN, as noted above, (b) ethanol is currently estimated, similar to Schroeder et al. (2020), and (c) R(VOC) in F0AM is low due to missing precursors. Like the higher PNs, highly reactive R(VOC) contributes a large portion of the PAN budget at high NO_x. The short-lived compounds contribute ~80% of PAN over SMA at the highest NO_x mixing ratios. At lower NO_x mixing ratios, moving away from SMA, longer-lived compounds, such as ethanol, contribute the most towards PAN production (~70%).

One of the interesting contributions not typically observed for PAN is MEK, which also contributes to PPN and PHAN. In prior studies, MEK mixing ratios were typically 0.5 to 2.0 ppbv (Bon et al., 2011; de Gouw et al., 2018; Liu et al., 2015). Over the SMA, 1.5 ppbv of MEK was observed on average with values as high as 8.3 ppbv. Due to the long lifetime of MEK (~30 hrs for the average photolysis rate measured and OH = 5×10^6 molec. cm^{-3}), the high mixing ratios of MEK are most likely due to direct emissions (e.g., de Gouw et al., 2005; Liu et al., 2015). Thus, there are potentially large sources of MEK in SMA that need to be considered in properly representing PAN chemistry.

https://doi.org/10.5194/egusphere-2024-596
Preprint. Discussion started: 2 April 2024

Another potentially important compound for PAN production is ethanol. However, this compound was not measured during KORUS-AQ; instead, it was estimated based on previous ground-based observations, similar to Schroeder et al. (2020). Ethanol is considered to mainly come from vehicle emissions (e.g., Millet et al., 2012) and potentially cleaning agents (e.g., McDonald et al., 2018). As ethanol use is predicted to increase in the future (e.g., de Gouw et al., 2012) and cleaning agents and other volatile chemical products appear to scale with population (Gkatzelis et al., 2021), ethanol and MEK may continue contributing towards the PAN budget in the SMA in the future.

As a note, two other compounds potentially important for PAN production that were not measured on the DC-8 during KORUS-AQ include methylglyoxal and biacetyl (LaFranchi et al., 2009). In a forested environment that was partially impacted by urban outflow, these two components contributed on average 25% of the PAN budget (LaFranchi et al., 2009). In urban environments, methylglyoxal is believed to mainly originate from aromatic oxidation (Ling et al., 2020); whereas, biacetyl is believed to come from anthropogenic emissions (Xu et al., 2023). Further, as discussed in Sect. 4.3, these two compounds may potentially be important missing HO_x sources, as well. Thus, measurements of these two compounds along with ethanol is necessary to better understand PAN chemistry.

4. Observational constraints of the HO_x and O_x budget over SMA

As highlighted in Figure S1, the three factors impacting instantaneous $P(O_x)$ are R(VOC), $P(HO_x)$, and NO_x loss processes. In Sect. 3, the NO_x loss processes were investigated and provided a constraint for R(VOC) to improve the investigation of $P(O_x)$. With R(VOC) constrained, the $RO_2^{\cdot}$ concentration can be estimated, providing a means to calculate the net $P(O_x)$ and to

https://doi.org/10.5194/egusphere-2024-596
Preprint. Discussion started: 2 April 2024

investigate the major reactions leading to O_x loss and total HO_x ($OH + HO_2 + RO_2^{\cdot} + R(O)O_2^{\cdot}$) loss. With the latter, this allows for an investigation of the major $P(HO_x)$ reactions, assuming $L(HO_x)$ equals $P(HO_x)$ (see Eq. 1 – 7 in Sect. 2.3).

4.1 Net O_x production and sources of O_x loss

Using the total R(VOC) from Sect. 3.3 (Figure 4a), the net $P(O_x)$ (Eq. 1 – 2) over SMA during KORUS-AQ has been determined (Figure 6a). The net $P(O_x)$ peaked at 10.3 ppbv hr^{-1} at ~8 ppbv NO_x. If only the measured and estimated R(VOC) from F0AM secondary products is used to calculate net $P(O_x)$, the value decreases to 8.8 ppbv hr^{-1}, but at the same NO_x mixing ratio. This value is similar to values observed in other urban locations around the world (~2 – 20 ppbv hr^{-1}), showing that many urban areas are still impacted by high $P(O_x)$ values (Brune et al., 2022; Griffith et al., 2016; Ma et al., 2022; Ren et al., 2013; Schroeder et al., 2020; Whalley et al., 2016, 2018).

The NO_x distribution over SMA (Figure 1) shows a large area (~127.53°E to 127.18°E, or ~39 km) is near the NO_x mixing ratio with the maximum $P(O_x)$ (Figure 6). Thus, a large portion of the SMA will have high instantaneous $P(O_x)$ of ~10 ppbv hr^{-1}. As the median wind speed over SMA during KORUS-AQ was ~5 m s^{-1}, an air parcel would remain at the highest $P(O_x)$ for ~2 hrs, leading to ~20 ppbv O_3 being produced (not including dilution). This agrees with the ~20 ppbv increase in O_3 observed over the Taehwa Research Forest supersite between midday and afternoon overpasses by the DC-8 during KORUS-AQ (Crawford et al., 2021). Thus, though there is a substantial O_3 background observed over SMA (Colombi et al., 2023; Crawford et al., 2021), a large contribution of the O_3 is due to photochemical production.

The major reactions leading to O_x loss ($L(O_x)$) are shown in Figure 6b. The two major reactions that lead to O_x loss are net R8 (light and dark red), or the net production of PNs (which

https://doi.org/10.5194/egusphere-2024-596
Preprint. Discussion started: 2 April 2024

includes losses), and R11, reaction of NO_2 with OH (blue) (see Table 1). Note, as discussed in Sect. 2.2, for the budget analysis conducted here, PAN and PPN were constrained to observations. At high NO_x (near emissions, ~30 ppbv), R11 (NO_2 + OH) dominates the $L(O_x)$ budget (> 60%), with net R8 (net PAN, dark red, and higher PNs, light red) contributing ~25%, and R12 – 14 accounting for the remaining 15% of O_x loss. As NO_x mixing ratios decrease (moving away from emissions), the net R8 reaction, producing both PAN and higher PNs, starts contributing to larger total $L(O_x)$, ranging from 30 – 40%. Furthermore, the net R8 reaction contribution towards $L(O_x)$ remains relatively constants with NO_x mixing ratios as the contribution from R11 (OH + NO_2) decreases. At NO_x mixing ratios < 3 ppbv is when non-NO_x reactions (R12 – 14) contribute greater than 30% of the $L(O_x)$ budget. Thus, proper representation of PAN and higher PNs, both in precursors and speciation, is important in properly understanding the O_x budget in SMA.

4.2 HO_x loss over the SMA

Similar to $L(O_x)$, the major reactions leading to $L(HO_x)$ over the SMA during KORUS-AQ were the reactions of NO_x with HO_x, specifically NO_2 with OH (R11) and net PAN (dark red) and higher PNs (light red) production (R8). Reaction R11 is most important for NO_x mixing ratios greater than 15 ppbv (50 – 65%). Between 5 and 15 ppbv, R11 is comparable to the net PN production (R8), where R11 comprises 35 – 50% of $L(HO_x)$ while net R8 (sum of higher $\sum$PNs and PAN) comprises 30 – 40% of $L(HO_x)$. At lower NO_x mixing ratios, R11 is always smaller for $L(HO_x)$ than net R8, where R11 is about a factor of 2 lower than net R8. Production of ΣANs played a minor role due to the low α_{eff}.

The self-reaction of HO_x species (R15 – R16) contributes minimally to $L(HO_x)$ (less than 10%) for NO_x mixing ratios greater than 8 ppbv. At lower NO_x mixing ratios, R16 starts

https://doi.org/10.5194/egusphere-2024-596
Preprint. Discussion started: 2 April 2024

dominating L(HO_x) budget, increasing from 8% at 8 ppbv to 50% of L(HO_x) at NO_x mixing ratios less than 2 ppbv. Reaction R15 remains relatively small for the L(HO_x) budget, only reaching 7% of the L(HO_x) budget at NO_x mixing ratios less than 2 ppbv.

4.3 Sources of HO_x over SMA

The analysis conducted leads to the ability to constrain HO_x losses over the SMA during KORUS-AQ. This is important as not all typical HO_x sources were measured on the DC-8 during the project (e.g., nitrous acid, or HONO), and HO_x production rates directly impacts P(O_x) (Figure S1). Prior studies (e.g., Griffith et al., 2016; Tan et al., 2019; Whalley et al., 2018) have demonstrated that in urban environments, sources of HO_x include photolysis of O_3 and subsequent reaction with water vapor, formaldehyde photolysis, and HONO photolysis. Furthermore, recent studies have highlighted the potential importance of typically non-measured OVOCs in their contribution to P(HO_x) and subsequent P(O_x) in an urban environment (Wang et al., 2022). To constrain the P(HO_x) over SMA during KORUS-AQ, the P(HO_x) was assumed to be equal to the observationally constrained L(HO_x). Then, P(HO_x) was calculated for the measurements on the DC-8, including photolysis of O_3, formaldehyde, H_2O_2, and other measured OVOCs (Table 2).

Comparing the calculated P(HO_x) and L(HO_x), ~1.5 ppbv hr^{-1} P(HO_x) (range 1.3 – 1.8 ppbv hr^{-1}) is not accounted for, leading to ~45% of the necessary L(HO_x) to maintain steady-state (Figure 7). For the calculated P(HO_x) budget, O_3 and formaldehyde photolysis contributed ~50% and 40% of the budget, respectively, with the remainder coming from photolysis of H_2O_2 and other measured OVOCs. Accounting for the unobserved P(HO_x), O_3 and formaldehyde photolysis contributed ~25% and ~20%, respectively.

https://doi.org/10.5194/egusphere-2024-596
Preprint. Discussion started: 2 April 2024

Potential missing sources of $P(HO_x)$ are briefly speculated here. First, one potential source is the photolysis of methylglyoxal. Using the F0AM predicted methylglyoxal, as it was not measured on the DC-8, methylglyoxal would contribute ~0.24 ppbv hr^{-1} $P(HO_x)$, or ~16% of the unobserved $P(HO_x)$. Another OVOC not measured on the DC-8 and expected to originate from anthropogenic emissions and not from chemistry is 2,3-butanedione, or biacetyl (de Gouw et al., 2018; Grosjean et al., 2002; Schauer et al., 2002; Xu et al., 2023; Zhou et al., 2020). Prior studies observed 20 – 400 pptv of biacetyl (de Gouw et al., 2018; Xu et al., 2023), correspond to 0.04 – 0.74 ppbv hr^{-1}, or 3 – 49% of the unobserved $P(HO_x)$. Thus, between these two OVOCs, 19 – 66% of the unobserved $P(HO_x)$ could be explained. Other unmeasured OVOCs could potentially contribute to the observed $P(HO_x)$ (e.g., Wang et al., 2022); however, there is less constraints both on the speciation and photolysis rates for these OVOCs (e.g., Mellouki et al., 2015). Finally, HONO could contribute to this observed $P(HO_x)$. Up to 700 pptv of HONO was observed in SMA during KORUS-AQ (Gil et al., 2021), though, this would quickly photolyze to the altitudes the DC-8 flew over SMA (Tuite et al., 2021). Even at 50 – 100 pptv HONO, photolysis of HONO would lead to 0.2 – 0.4 ppbv hr^{-1} $P(HO_x)$, or 13 – 27% of the unobserved $P(HO_x)$. Thus, between methylglyoxal, biacetyl, and HONO, between 32 – 92% of the unobserved $P(HO_x)$ could be accounted for. This analysis highlights the importance of measuring these HO_x sources to better understand and constrain O_x chemistry in SMA and other urban environments.

One note about this analysis is that particulate matter collected onto the downwelling CAFS optics during KORUS-AQ (see Sect. S5, Table S3, and Figure S11). Corrections of up to 20% were determined, and the associated uncertainties were also increased by 20% due to the corrections. Thus, the exact amount of unmeasured $P(HO_x)$ is potentially smaller than discussed.

https://doi.org/10.5194/egusphere-2024-596
Preprint. Discussion started: 2 April 2024

5. Conclusions and Implications

In the Seoul Metropolitan Area (SMA), the ozone (O_3) mixing ratio often exceeds current standards and is increasing. Many processes can impact the O_3 mixing ratios and exceedances. Here, the processes that impact instantaneous O_3 production ($P(O_x)$, where O_x is O_3 + NO_2 to account for possible O_3 titration) were investigated for observations collected on the NASA DC-8 during the 2016 NIER/NASA Korea United-States Air Quality (KORUS-AQ) study. The observations indicate missing oxidized NO_x products (NO_z) that include both the short-lived peroxy nitrates (ΣPNs) and alkyl and multi-functional nitrates (ΣANs). ΣPNs contributed the most for the organic NO_z species. Only ~50% of the ΣPNs were speciated over SMA, which is atypical as prior studies typically show closure between the speciated and total PN measurements.

The un-speciated ΣPNs and ΣANs were used to constrain the missing volatile organic compound (VOC) reactivity (R(VOC)), as R(VOC) is important in constraining the instantaneous $P(O_3)$. The missing R(VOC) was found to be 1.4 to 2.1 s^{-1}. The F0AM box model further supports the role of unmeasured ΣPNs as an important temporary NO_x and radical sink over SMA. F0AM predicts ~50% of the higher ΣPNs (higher ΣPNs = ΣPNs – PAN), indicating missing R(VOCs) may explain the other 50%. Constraints from both the ΣPNs and ΣANs suggest that this missing R(VOC) would include oxygenated VOCs (OVOCs), including aldehydes such as octanal and nonanal from cooking, and alkenes from anthropogenic emissions.

With the constraints on the R(VOC), the net instantaneous $P(O_x)$ was determined for SMA. It was found to peak at ~10 ppbv hr^{-1} at ~8 ppbv NO_x. A large fraction of the SMA area was, on average, at this mixing ratio of NO_x, indicating high local $P(O_x)$. This supports the increase of ~20 ppbv of O_3 observed in a downwind site (Taehwa Research Forest supersite) from midday to afternoon during KORUS-AQ.

https://doi.org/10.5194/egusphere-2024-596
Preprint. Discussion started: 2 April 2024

With the comprehensive measurements on-board the DC-8, the F0AM model results, and the observationally constrained R(VOC), a budget analysis on the sinks of O_3 ($L(O_x)$) and HO_x ($L(HO_x)$, where $HO_x = OH + HO_2 + RO_2^{\cdot} + R(O)O_2^{\cdot}$) was performed. Due to the high R(VOC), type of VOC, and the NO_2-to-NO ratio, net ΣPNs production is surprisingly a large and important sink of O_x and HO_x over SMA (~25 – 40% and 15 – 40% for $L(O_x)$ and $L(HO_x)$, respectively), with production of HNO_3 and radical self-reactions accounting for the other $L(O_x)$ and $L(HO_x)$ losses. Net ΣPNs production as an important $L(O_x)$ and $L(HO_x)$ term is significant, as ΣPNs is a temporary reservoir of both NO_2 and $R(O)O_2^{\cdot}$ but has not traditionally been included in these calculations. Downwind locations separated from the local NO_x and VOC emissions of the SMA will experience increased $P(O_x)$ due to the release of NO_2 and $R(O)O_2^{\cdot}$. With the constraint of $L(HO_x)$, $P(HO_x)$ was investigated, assuming steady-state, and unmeasured HONO plus unmeasured OVOCs were found to be necessary to explain the missing HO_x sources. Both sources of HO_x are either missing or highly uncertain in chemical transport models.

Though the high regional background and foreign sources of O_3 and its precursors elevate the O_3 levels in SMA and potentially already causes the SMA to be in exceedance for O_3 concentrations, this study highlights the importance local, in-situ $P(O_x)$ to the SMA area, which can further exacerbate the O_3 concentrations for SMA and the surrounding region. The results support the observations of increasing O_3 with decreasing NO_x that has been observed for SMA in prior studies. Further, the study highlights the important role of unmeasured VOCs and OVOCs and the necessity to understand their sources and role in NO_x and O_3 chemistry. Further, the study demonstrates the interplay of direct emissions or secondary production of PN precursors and its role in net $P(O_x)$. Attempts at specifically reducing the sources of PN may adversely impact net $P(O_x)$, as lower net PN chemistry may increase O_3 due to more NO_2 being available.

https://doi.org/10.5194/egusphere-2024-596
Preprint. Discussion started: 2 April 2024

Competing Interests

At least one of the (co-)authors is a member of the editorial board of Atmospheric Chemistry and Physics.

Acknowledgements

The authors acknowledge Michelle Kim, Alex Teng, John Crounse, and Paul O. Wennberg for their measurements with CIT-CIMS (HNO_3, multifunctional alkyl nitrates, and OVOCs), William H. Brune for his measurements with ATHOS (OH, OH reactivity), Alan Fried for his measurements with CAMS (CH_2O and C_2H_6), Paul Romer-Present for his contribution to collecting data with TD-LIF, Sally Pusede for her contributions to collecting data with DACOM and DLH, and Andrew J. Weinheimer for his measurements of NO, O_3, and NO_y. The PTR-MS instrument team (P. Eichler, L. Kaser, T. Mikoviny, M. Müller) are acknowledged for their support.

Funding

BAN and KRT acknowledge NASA grant 80NSSC22K0283. LGH and YL acknowledge NASA grant NNX15AT90G for the PAN measurements. SRH and KU were supported by NASA grant NNX15AT99G for photolysis measurements. AW acknowledges support by the Austrian Federal Ministry for Transport, Innovation, and Technology (bmvit-FFG-ASA) for the PTR-MAS measurements. PCJ and JLJ were supported by NASA 80NSSC21K1451 and 80NSSC23K0828.

Data Availability

https://doi.org/10.5194/egusphere-2024-596
Preprint. Discussion started: 2 April 2024

Version R6 1-min merged data used in this analysis available at DOI:10.5067/Suborbital/KORUSAQ/DATA01. The F0AM setup file, input file, and output files are all available at https://doi.org/10.5281/zenodo.10723227.

Author Contribution

BAN, KRT, and JHC designed the experiment and wrote the paper. BAN and KRT analyzed the data. KRT ran the F0AM model and KRT and BAN analyzed the model output. BAN, DRB, PCJ, RCC, JPD, GSD, SRH, LGH, JLJ, K-EK, YL, IJS, KU, and AW collected and QA/QC the data during KORUS-AQ. All authors contributed to the writing and editing of the paper.

https://doi.org/10.5194/egusphere-2024-596
Preprint. Discussion started: 2 April 2024

References

Archibald, A. T., Neu, J. L., Elshorbany, Y. F., Cooper, O. R., Young, P. J., Akiyoshi, H., Cox, R. A., Coyle, M., Derwent, R. G., Deushi, M., Finco, A., Frost, G. J., Galbally, I. E., Gerosa, G., Granier, C., Griffiths, P. T., Hossaini, R., Hu, L., Jöckel, P., Josse, B., Lin, M. Y., Mertens, M., Morgenstern, O., Naja, M., Naik, V., Oltmans, S., Plummer, D. A., Revell, L. E., Saiz-Lopez, A., Saxena, P., Shin, Y. M., Shahid, I., Shallcross, D., Tilmes, S., Trickl, T., Wallington, T. J., Wang, T., Worden, H. M., and Zeng, G.: Tropospheric ozone assessment report: A critical review of changes in the tropospheric ozone burden and budget from 1850 to 2100, https://doi.org/10.1525/elementa.2020.034, 2020.

Atkinson, R.: Kinetics of the gas-phase reactions of OH radicals with alkanes and cycloalkanes, Atmos Chem Phys, 3, 2233–2307, https://doi.org/10.5194/acp-3-2233-2003, 2003.

Atkinson, R. and Arey, J.: Atmospheric Degradation of Volatile Organic Compounds, Chem Rev, 103, 4605–4638, https://doi.org/10.1021/CR0206420, 2003.

Atkinson, R., Baulch, D. L., Cox, R. A., Crowley, J. N., Hampson, R. F., Hynes, R. G., Jenkin, M. E., Rossi, M. J., and Troe, J.: Evaluated kinetic and photochemical data for atmospheric chemistry: Volume II - gas phase reactions of organic species, Atmos Chem Phys, 6, 3625–4055, https://doi.org/10.5194/acp-6-3625-2006, 2006.

Bohn, B. and Zetzsch, C.: Kinetics and mechanism of the reaction of OH with the trimethylbenzenes – experimental evidence for the formation of adduct isomers, Physical Chemistry Chemical Physics, 14, 13933, https://doi.org/10.1039/c2cp42434g, 2012.

Bon, D. M., Ulbrich, I. M., De Gouw, J. a., Warneke, C., Kuster, W. C., Alexander, M. L., Baker, a., Beyersdorf, a. J., Blake, D., Fall, R., Jimenez, J. L., Herndon, S. C., Huey, L. G., Knighton, W. B., Ortega, J., Springston, S., and Vargas, O.: Measurements of volatile organic compounds at a suburban ground site (T1) in Mexico City during the MILAGRO 2006 campaign: measurement comparison, emission ratios, and source attribution, Atmos Chem Phys, 11, 2399–2421, https://doi.org/10.5194/acp-11-2399-2011, 2011.

Bourgeois, I., Peischl, J., Neuman, J. A., Brown, S. S., Allen, H. M., Campuzano-jost, P., Coggon, M. M., Digangi, J. P., Diskin, G. S., Gilman, J. B., Gkatzelis, G. I., Guo, H., Halliday, H. A., Hanisco, T. F., Holmes, C. D., Nault, B. A., Nowak, J. B., Pagonis, D., Rickly, P. S., Robinson, M. A., Veres, P. R., Warneke, C., Wennberg, P. O., Washenfelder, R. A., and Wiggins, E. B.: Comparison of airborne measurements of NO, NO_2, HONO, NO_y, and CO during FIREX-AQ, Atmos Meas Tech, 15, 4901–4930, https://doi.org/10.5194/amt-15-4901-2022, 2022.

Brune, W. H., Miller, D. O., Thames, A. B., Allen, H. M., Apel, E. C., Blake, D. R., and Bui, T. P.: Exploring Oxidation in the Remote Free Troposphere : Insights From Atmospheric Tomography (ATom), Journal of Geophysical Research : Atmospheres, 125, c2019JD031685, https://doi.org/10.1029/2019JD031685, 2019.

Brune, W. H., Miller, D. O., Thames, A. B., Brosius, A. L., Barletta, B., Blake, D. R., Blake, N. J., Chen, G., Choi, Y., Crawford, J. H., Digangi, J. P., Diskin, G., Fried, A., Hall, S. R., Hanisco, T. F., Huey, G. L., Hughes, S. C., Kim, M., Meinardi, S., Montzka, D. D., Pusede, S. E., Schroeder, J. R., Teng, A., Tanner, D. J., Ullmann, K., Walega, J., Weinheimer, A., Wisthaler, A., and Wennberg, P. O.: Observations of atmospheric oxidation and ozone production in South Korea, Atmos Environ, 269, 118854, https://doi.org/10.1016/j.atmosenv.2021.118854, 2022.

https://doi.org/10.5194/egusphere-2024-596
Preprint. Discussion started: 2 April 2024

766 Burkholder, J. B., Sander, S. P., Abbatt, J. P. D., Barker, J. R., Cappa, C. D., Crounse, J. D., Dibble,
767 T. S., Huie, R. E., Kolb, C. E., Kurylo, M. J., Orkin, V. L., Percival, C. J., Wilmouth, D. M., and
768 Wine, P. H.: Chemical Kinetics and Photochemical Data for Use in Atmospheric Studies,
769 Evaluation No. 19, Pasadena, CA, USA, 2020.

770 Coggon, M. M., Stockwell, C. E., Claflin, M. S., Pfannerstill, E. Y., Lu, X., Gilman, J. B.,
771 Marcantonio, J., Cao, C., Bates, K., Gkatzelis, G. I., Lamplugh, A., Katz, E. F., Arata, C., Apel, E.
772 C., Hornbrook, R. S., Piel, F., Majluf, F., Blake, D. R., Wisthaler, A., Canagaratna, M., Lerner, B.
773 M., Goldstein, A. H., Mak, J. E., and Warneke, C.: Identifying and correcting interferences to
774 PTR-ToF- MS measurements of isoprene and other urban volatile organic compounds, Atmos
775 Meas Tech, 17, 801–825, https://doi.org/10.5194/amt-17-801-2024, 2024.

776 Cohen, A. J., Brauer, M., Burnett, R., Anderson, H. R., Frostad, J., Estep, K., Balakrishnan, K.,
777 Brunekreef, B., Dandona, L., Dandona, R., Feigin, V., Freedman, G., Hubbell, B., Jobling, A.,
778 Kan, H., Knibbs, L., Liu, Y., Martin, R., Morawska, L., Pope, C. A., Shin, H., Straif, K., Shaddick,
779 G., Thomas, M., van Dingenen, R., van Donkelaar, A., Vos, T., Murray, C. J. L., and Forouzanfar,
780 M. H.: Estimates and 25-year trends of the global burden of disease attributable to ambient air
781 pollution: an analysis of data from the Global Burden of Diseases Study 2015, The Lancet, 389,
782 1907–1918, https://doi.org/10.1016/S0140-6736(17)30505-6, 2017.

783 Colombi, N. K., Jacob, D. J., Yang, L. H., Zhai, S., Shah, V., Grange, S. K., Yantosca, R. M., Kim,
784 S., and Liao, H.: Why is ozone in South Korea and the Seoul metropolitan area so high and
785 increasing?, Atmos Chem Phys, 23, 4031–4044, https://doi.org/10.5194/acp-23-4031-2023, 2023.

786 Crawford, J. H., Ahn, J. Y., Al-Saadi, J., Chang, L., Emmons, L. K., Kim, J., Lee, G., Park, J. H.,
787 Park, R. J., Woo, J. H., Song, C. K., Hong, J. H., Hong, Y. D., Lefer, B. L., Lee, M., Lee, T., Kim,
788 S., Min, K. E., Yum, S. S., Shin, H. J., Kim, Y. W., Choi, J. S., Park, J. S., Szykman, J. J., Long,
789 R. W., Jordan, C. E., Simpson, I. J., Fried, A., Dibb, J. E., Cho, S. Y., and Kim, Y. P.: The Korea-
790 United States air quality (KORUS-AQ) field study, Elementa, 9, 1–27,
791 https://doi.org/10.1525/elementa.2020.00163, 2021.

792 Crounse, J., McKinney, K. A., Kwan, A. J., and Wennberg, P. O.: Measurement of gas-phase
793 hydroperoxides by chemical ionization mass spectrometry, Anal Chem, 78, 6726–6732,
794 https://doi.org/doi:10.1021/ac0604235, 2006.

795 Day, D. A., Wooldridge, P. J., Dillon, M. B., Thornton, J. A., and Cohen, R. C.: A thermal
796 dissociation laser-induced fluorescence instrument for in situ detection of NO_2, peroxy nitrates,
797 alkyl nitrates, and HNO_3, Journal of Geophysical Research-Atmospheres, 107, 4046,
798 https://doi.org/10.1029/2001JD000779, 2002.

799 Day, D. A., Campuzano-Jost, P., Nault, B. A., Palm, B. B., Hu, W., Guo, H., Wooldridge, P. J.,
800 Cohen, R. C., Docherty, K. S., Huffman, J. A., De Sá, S. S., Martin, S. T., and Jimenez, J. L.: A
801 systematic re-evaluation of methods for quantification of bulk particle-phase organic nitrates using
802 real-Time aerosol mass spectrometry, Atmos Meas Tech, 15, 459–483,
803 https://doi.org/10.5194/amt-15-459-2022, 2022.

804 Diskin, G. S., Podolske, J. R., Sachse, G. W., and Slate, T. A.: Open-path airborne tunable diode
805 laser hygrometer, in: Diode Lasers and Applications in Atmospheric Sensing, edited by: Fried, A.,
806 Proceedings of the Society of Photo-Optical Instrumentation Engineers (SPIE), 4817, 196–204,
807 https://doi.org/doi:10.1117/12.453736, 2002.

https://doi.org/10.5194/egusphere-2024-596
Preprint. Discussion started: 2 April 2024

Espada, C. and Shepson, P. B.: The production of organic nitrates from atmospheric oxidation of ethers and glycol ethers, Int J Chem Kinet, 37, 686–699, https://doi.org/10.1002/kin.20121, 2005.

Faloona, I. C., Tan, D., Lesher, R. L., Hazen, N. L., Frame, C. L., Simpas, J. B., Harder, H., Martinez, M., Di Carlo, P., Ren, X., and Brune, W. H.: A Laser-induced Fluorescence Instrument for Detecting Tropospheric OH and HO_2 : Characteristics and Calibration, J Atmos Chem, 47, 139–167, https://doi.org/10.1023/B:JOCH.0000021036.53185.0e, 2004.

Farmer, D. K., Perring, A. E., Wooldridge, P. J., Blake, D. R., Baker, A., Meinardi, S., Huey, L. G., Tanner, D., Vargas, O., and Cohen, R. C.: Impact of organic nitrates on urban ozone production, Atmos Chem Phys, 11, 4085–4094, https://doi.org/10.5194/acp-11-4085-2011, 2011.

Fisher, J. A., Jacob, D. J., Travis, K. R., Kim, P. S., Marais, E. A., Miller, C. C., Yu, K., Zhu, L., Yantosca, R. M., Sulprizio, M. P., Mao, J., Wennberg, P. O., Crounse, J. D., Teng, A. P., Nguyen, T. B., Clair, J. M. S., Cohen, R. C., Romer, P., Nault, B. A., Wooldridge, P. J., Jimenez, J. L., Campuzano-Jost, P., Day, D. A., Hu, W., Shepson, P. B., Xiong, F., Blake, D. R., Goldstein, A. H., Misztal, P. K., Hanisco, T. F., Wolfe, G. M., Ryerson, T. B., Wisthaler, A., and Mikoviny, T.: Organic nitrate chemistry and its implications for nitrogen budgets in an isoprene- and monoterpene-rich atmosphere: Constraints from aircraft ($SEAC^4RS$) and ground-based (SOAS) observations in the Southeast US, Atmos Chem Phys, 16, https://doi.org/10.5194/acp-16-5969-2016, 2016.

Fried, A., Walega, J., Weibring, P., Richter, D., Simpson, I. J., Blake, D. R., Blake, N. J., Meinardi, S., Barletta, B., Hughes, S. C., Crawford, J. H., Diskin, G., Barrick, J., Hair, J., Fenn, M., Wisthaler, A., Mikoviny, T., Woo, J., Park, M., Kim, J., Min, K., Jeong, S., Wennberg, P. O., Kim, M. J., Crounse, J. D., Teng, A. P., Bennett, R., Yang-martin, M., Shook, M. A., Huey, G., Tanner, D., Knote, C., and Kim, J.: Airborne formaldehyde and volatile organic compound measurements over the Daesan petrochemical complex on Korea's northwest coast during the Korea-United States Air Quality study : Estimation of emission fluxes and effects on air quality, Elementa: Science of the Anthropocene, 8, 1, https://doi.org/10.1525/elementa.2020.121, 2020.

Galloway, M. M., Huisman, A. J., Yee, L. D., Chan, A. W. H., Loza, C. L., Seinfeld, J. H., and Keutsch, F. N.: Yields of oxidized volatile organic compounds during the OH radical initiated oxidation of isoprene, methyl vinyl ketone, and methacrolein under high-NO_x conditions, Atmos Chem Phys, 11, https://doi.org/10.5194/acp-11-10779-2011, 2011.

Gaudel, A., Cooper, O. R., Ancellet, G., Barret, B., Boynard, A., Burrows, J. P., Clerbaux, C., Coheur, P. F., Cuesta, J., Cuevas, E., Doniki, S., Dufour, G., Ebojie, F., Foret, G., Garcia, O., Granados-Muñoz, M. J., Hannigan, J. W., Hase, F., Hassler, B., Huang, G., Hurtmans, D., Jaffe, D., Jones, N., Kalabokas, P., Kerridge, B., Kulawik, S., Latter, B., Leblanc, T., Le Flochmoën, E., Lin, W., Liu, J., Liu, X., Mahieu, E., McClure-Begley, A., Neu, J. L., Osman, M., Palm, M., Petetin, H., Petropavlovskikh, I., Querel, R., Rahpoe, N., Rozanov, A., Schultz, M. G., Schwab, J., Siddans, R., Smale, D., Steinbacher, M., Tanimoto, H., Tarasick, D. W., Thouret, V., Thompson, A. M., Trickl, T., Weatherhead, E., Wespes, C., Worden, H. M., Vigouroux, C., Xu, X., Zeng, G., and Ziemke, J.: Tropospheric Ozone Assessment Report: Present-day distribution and trends of tropospheric ozone relevant to climate and global atmospheric chemistry model evaluation, Elementa, 6, https://doi.org/10.1525/elementa.291, 2018.

Gil, J., Kim, J., Lee, M., Lee, G., Ahn, J., Soo, D., Jung, J., Cho, S., Whitehill, A., Szykman, J., and Lee, J.: Characteristics of HONO and its impact on O_3 formation in the Seoul Metropolitan

https://doi.org/10.5194/egusphere-2024-596
Preprint. Discussion started: 2 April 2024

Area during the Korea-US Air Quality study, Atmos Environ, 247, 118182, https://doi.org/10.1016/j.atmosenv.2020.118182, 2021.

Gkatzelis, G. I., Coggon, M. M., Mcdonald, B. C., Peischl, J., Aikin, K. C., Gilman, J. B., Trainer, M., and Warneke, C.: Identifying Volatile Chemical Product Tracer Compounds in U.S. Cities, Enviromental Science & Technology, 55, 188–199, https://doi.org/10.1021/acs.est.0c05467, 2021.

González-Sánchez, J. M., Brun, N., Wu, J., Ravier, S., and Clément, J.: On the importance of multiphase photolysis of organic nitrates on their global atmospheric removal, Atmos Chem Phys, 23, 5851–5866, https://doi.org/10.5194/acp-23-5851-2023, 2023.

de Gouw, J. A., Middlebrook, A. M., Warneke, C., Goldan, P. D., Kuster, W. C., Roberts, J. M., Fehsenfeld, F. C., Worsnop, D. R., Canagaratna, M. R., Pszenny, A. A. P., Keene, W. C., Marchewka, M. L., Bertman, S. B., and Bates, T. S.: Budget of organic carbon in a polluted atmosphere: Results from the New England Air Quality Study in 2002, Journal of Geophysical Research: Atmospheres, 110, D16305, https://doi.org/10.1029/2004JD005623, 2005.

de Gouw, J. A., Gilman, J. B., Borbon, A., Warneke, C., Kuster, W. C., Goldan, P. D., Holloway, J. S., Peischl, J., Ryerson, T. B., Parrish, D. D., Gentner, D. R., Goldstein, A. H., and Harley, R. A.: Increasing atmospheric burden of ethanol in the United States, Geophys Res Lett, 39, L15803, https://doi.org/10.1029/2012GL052109, 2012.

de Gouw, J. A., Gilman, J. B., Kim, S.-W., Alvarez, S. L., Dusanter, S., Graus, M., Griffith, S. M., Isaacman-VanWertz, G., Kuster, W. C., Lefer, B. L., Lerner, B. M., McDonald, B. C., Rappenglück, B., Roberts, J. M., Stevens, P. S., Stutz, J., Thalman, R., Veres, P. R., Volkamer, R., Warneke, C., Washenfelder, R. A., and Young, C. J.: Chemistry of Volatile Organic Compounds in the Los Angeles Basin: Formation of Oxygenated Compounds and Determination of Emission Ratios, Journal of Geophysical Research: Atmospheres, 123, 2298–2319, https://doi.org/10.1002/2017JD027976, 2018.

Griffith, S. M., Hansen, R. F., Dusanter, S., Michoud, V., Gilman, J. B., Kuster, W. C., Veres, P. R., Graus, M., de Gouw, J. A., Roberts, J., Young, C., Washenfelder, R., Brown, S. S., Thalman, R., Waxman, E., Volkamer, R., Tsai, C., Stutz, J., Flynn, J. H., Grossberg, N., Lefer, B., Alvarez, S. L., Rappenglueck, B., Mielke, L. H., Osthoff, H. D., and Stevens, P. S.: Measurements of hydroxyl and hydroperoxy radicals during CalNex-LA: Model comparisons and radical budgets, Journal of Geophysical Research: Atmospheres, 121, 4211–4232, https://doi.org/10.1002/2015JD024358, 2016.

Grosjean, D., Grosjean, E., and Gertler, A. W.: On-Road Emissions of Carbonyls from Light-Duty and Heavy-Duty Vehicles, Enviromental Science & Technology, 35, 45–53, https://doi.org/10.1021/es001326a, 2002.

Hansen, R. F., Griffith, S. M., Dusanter, S., Gilman, J. B., Graus, M., Kuster, W. C., Veres, P. R., de Gouw, J. A., Warneke, C., Washenfelder, R. A., Young, C. J., Brown, S. S., Alvarez, S. L., Flynn, J. H., Grossberg, N. E., Lefer, B., Rappenglueck, B., and Stevens, P. S.: Measurements of Total OH Reactivity During CalNex-LA, Journal of Geophysical Research: Atmospheres, 126, e2020JD032988, https://doi.org/10.1029/2020JD032988, 2021.

Hurst Bowman, J., Barket, D. J., and Shepson, P. B.: Atmospheric chemistry of nonanal, Enviromental Science & Technology, 37, 2218–2225, 2003.

https://doi.org/10.5194/egusphere-2024-596
Preprint. Discussion started: 2 April 2024

892 Jenkin, M. E., Young, J. C., and Rickard, A. R.: The MCM v3.3.1 degradation scheme for isoprene,
893 Atmos Chem Phys, 15, 11433–11459, https://doi.org/10.5194/acp-15-11433-2015, 2015.

894 Jo, D. S., Emmons, L. K., Callaghan, P., Tilmes, S., and Woo, J.: Comparison of Urban Air Quality
895 Simulations During the KORUS-AQ Campaign With Regionally Refined Versus Global Uniform
896 Grids in the Multi-Scale Infrastructure for Chemistry and Aerosols (MUSICA) Version 0, J Adv
897 Model Earth Syst, 15, e2022MS003458, https://doi.org/10.1029/2022MS003458, 2023.

898 Jordan, C. E., Crawford, J. H., Beyersdorf, A. J., Eck, T. F., Halliday, H. S., Nault, B. A., Chang,
899 L. S., Park, J. S., Park, R., Lee, G., Kim, H., Ahn, J. Y., Cho, S., Shin, H. J., Lee, J. H., Jung, J.,
900 Kim, D. S., Lee, M., Lee, T., Whitehill, A., Szykman, J., Schueneman, M. K., Campuzano-Jost,
901 P., Jimenez, J. L., DiGangi, J. P., Diskin, G. S., Anderson, B. E., Moore, R. H., Ziemba, L. D.,
902 Fenn, M. A., Hair, J. W., Kuehn, R. E., Holz, R. E., Chen, G., Travis, K., Shook, M., Peterson, D.
903 A., Lamb, K. D., and Schwarz, J. P.: Investigation of factors controlling PM2.5 variability across
904 the South Korean Peninsula during KORUS-AQ, Elementa, 8,
905 https://doi.org/10.1525/elementa.424, 2020.

906 Kenagy, H. S., Sparks, T. L., Ryerson, T. B., Blake, D. R., and Cohen, R. C.: Evidence of
907 Nighttime Production of Organic Nitrates During SEAC^{4}RS, FRAPPE, and KORUS-AQ,
908 Geophys Res Lett, 47, e2020GL087860, https://doi.org/10.1029/2020GL087860, 2020.

909 Kenagy, H. S., Romer Present, P. S., Wooldridge, P. J., Nault, B. A., Campuzano-Jost, P., Day, D.
910 A., Jimenez, J. L., Zare, A., Pye, H. O. T., Yu, J., Song, C. H., Blake, D. R., Woo, J. H., Kim, Y.,
911 and Cohen, R. C.: Contribution of Organic Nitrates to Organic Aerosol over South Korea during
912 KORUS-AQ, Environ Sci Technol, 55, 16326–16338, https://doi.org/10.1021/acs.est.1c05521,
913 2021.

914 Kim, D., Cho, C., Jeong, S., Lee, S., Nault, B. A., Campuzano-jost, P., Day, D. A., Schroder, J.
915 C., Jimenez, J. L., Volkamer, R., Pusede, S. E., Hall, S. R., Ullmann, K., Huey, L. G., Tanner, D.
916 J., and Dibb, J.: Field observational constraints on the controllers in glyoxal (CHOCHO) reactive
917 uptake to aerosol, Atmos Chem Phys, 22, 805–821, https://doi.org/10.5194/acp-22-805-2022,
918 2022a.

919 Kim, H., Zhang, Q., and Heo, J.: Influence of Intense secondary aerosol formation and long-range
920 transport on aerosol chemistry and properties in the Seoul Metropolitan Area during spring time :
921 Results from KORUS-AQ, Atmos. Chem. Phys., 18, 7149–7168, https://doi.org/10.51944/acp-
922 2017-947, 2018.

923 Kim, H., Park, R. J., Kim, S., Brune, W. H., Diskin, G. S., Fried, A., Hall, S. R., Weinheimer, A.
924 J., Wennberg, P., Wisthaler, A., Blake, D. R., and Ullmann, K.: Observed versus simulated OH
925 reactivity during KORUS-AQ campaign : Implications for emission inventory and chemical
926 environment in East Asia, Elementa, 10, 1–26, 2022b.

927 Kim, J., Lee, J., Han, J., Choi, J., Kim, D.-G., Park, J., and Lee, G.: Long-term Assessment of
928 Ozone Nonattainment Changes in South Korea Compared to US, and EU Ozone Guidelines, Asian
929 Journal of Atmospheric Environment, 15, 20–32, https://doi.org/10.5572/ajae.2021.098, 2021.

930 Kim, S., Huey, L. G., Stickel, R. E., Tanner, D. J., Crawford, J. H., Olson, J. R., Chen, G., Brune,
931 W. H., Ren, X., Lesher, R., Wooldridge, P. J., Bertram, T. H., Perring, A., Cohen, R. C., Lefer, B.
932 L., Shetter, R. E., Avery, M., Diskin, G., and Sokolik, I.: Measurement of HO2NO2 in the free
933 troposphere during the Intercontinental Chemical Transport Experiment–North America 2004,

Journal of Geophysical Research: Atmospheres, 112, D12S01, https://doi.org/10.1029/2006JD007676, 2007.

Kim, S., Sanchez, D., Wang, M., Seco, R., Jeong, D., Hughes, S., Barletta, B., Blake, D. R., Jung, J., Kim, D., Lee, G., Lee, M., Ahn, J., Lee, S.-D., Cho, G., Sung, M.-Y., Lee, Y.-H., Kim, D. B., Kim, Y., Woo, J.-H., Jo, D., Park, R., Park, J.-H., Hong, Y.-D., Hong, J.-H., Zhang, D. Y., Liu, J. J., Li, B. J., Davis, D. L., Bell, M. L., Fletcher, T., Haagen-Smit, A. J., Blacet, F. E., Edinger, J. G., Yum, S. S., Roberts, G., Kim, J. H., Song, K. Y., Kim, D. Y., Lim, Y. J., Armendariz, A., Son, Y. S., Kim, J. C., Kim, S., Kim, S. Y., Lee, M., Shim, H., Wolfe, G. M., Guenther, A. B., He, A., Hong, Y., Han, J., Kim, S., Lee, M., Kim, S., Choi, S., Seok, S., Kim, S., Kim, S. Y., Jiang, X. Y., Lee, M., Turnipseed, A., Guenther, A., Kim, J. C., Lee, S. J., Kim, S., Lee, K. Y., Kwak, K. H., Ryu, Y. H., Lee, S. H., Baik, J. J., Ryu, Y. H., Baik, J. J., Kwak, K. H., Kim, S., Moon, N., Bao, H., Shrestha, K. L., Kondo, A., Kaga, A., Inoue, Y., Ran, L., Zhao, C. S., Xu, W. Y., Lu, X. Q., Han, M., Lin, W. L., Yan, P., Xu, X. B., Deng, Z. Z., Ma, N., Liu, P. F., Yu, J., Liang, W. D., Chen, L. L., Geng, F., Tie, X., Guenther, A., Li, G., et al.: OH reactivity in urban and suburban regions in Seoul, South Korea – an East Asian megacity in a rapid transition, Faraday Discuss., 189, 231–251, https://doi.org/10.1039/C5FD00230C, 2016.

KORUS-AQ Science Team: KORUS-AQ Data, [Dataset], NASA Langley Research Center., https://doi.org/10.5067/Suborbital/KORUSAQ/DATA01, 2023.

LaFranchi, B. W., Wolfe, G. M., Thornton, J. a., Harrold, S. a., Browne, E. C., Min, K. E., Wooldridge, P. J., Gilman, J. B., Kuster, W. C., Goldan, P. D., DeGouw, J. a., McKay, M., Goldstein, a. H., Ren, X. R., Mao, J. Q., Cohen, R. C., de Gouw, J. a., Welsh-Bon, D., Chen, Z., and Brune, W. H.: Closing the peroxy acetyl (PA) radical budget: Observations of acyl peroxy nitrates (PAN, PPN and MPAN) during BEARPEX 2009, Abstracts of Papers of the American Chemical Society, 9, 289, https://doi.org/10.5194/acp-9-7623-2009, 2009.

Lee, Y. R., Huey, L. G., Tanner, D. J., Takeuchi, M., Qu, H., Liu, X., Ng, N. L., Crawford, J. H., Fried, A., Richter, D., Simpson, I. J., Blake, D. R., Blake, N. J., Meinardi, S., Kim, S., Diskin, G. S., Digangi, J. P., Choi, Y., Pusede, S. E., Wennberg, P. O., Kim, M. J., Crounse, J. D., Teng, A. P., Cohen, R. C., Romer, P. S., Brune, W., Wisthaler, A., Mikoviny, T., Jimenez, J. L., Campuzano-Jost, P., Nault, B. A., Weinheimer, A., Hall, S. R., and Ullmann, K.: An investigation of petrochemical emissions during KORUS-AQ: Ozone production, reactive nitrogen evolution, and aerosol production, Elementa, 10, 1–24, https://doi.org/10.1525/elementa.2022.00079, 2022.

Ling, Z., Xie, Q., Shao, M., Wang, Z., Wang, T., Guo, H., and Wang, X.: Formation and sink of glyoxal and methylglyoxal in a polluted subtropical environment: Observation-based photochemical analysis and impact evaluation, Atmos Chem Phys, 20, 11451–11467, https://doi.org/10.5194/acp-20-11451-2020, 2020.

Liu, Y., Yuan, B., Li, X., Shao, M., Lu, S., Li, Y., Chang, C., Wang, Z., Hu, W., Huang, X., He, L., Zeng, L., Hu, M., and Zhu, T.: Impact of pollution controls in Beijing on atmospheric oxygenated volatile organic compounds (OVOCs) during the 2008 Olympic Games : observation and modeling implications, Atmos Chem Phys, 15, 3045–3062, https://doi.org/10.5194/acp-15-3045-2015, 2015.

Lyu, X. P., Zeng, L. W., Guo, H., Simpson, I. J., Ling, Z. H., Wang, Y., Murray, F., Louie, P. K. K., Saunders, S. M., Lam, S. H. M., and Blake, D. R.: Evaluation of the effectiveness of air

pollution control measures in Hong Kong, Environmental Pollution, 220, 87–94, https://doi.org/10.1016/j.envpol.2016.09.025, 2017.

Ma, P. K., Zhao, Y., Robinson, A. L., Worton, D. R., Goldstein, A. H., Ortega, A. M., Jimenez, J.-L., Zotter, P., Prévôt, A. S. H., Szidat, S., and Hayes, P. L.: Evaluating the impact of new observational constraints on P-S/IVOC emissions, multi-generation oxidation, and chamber wall losses on SOA modeling for Los Angeles, CA, Atmos Chem Phys, 17, 9237–9259, https://doi.org/10.5194/acp-17-9237-2017, 2017.

Ma, X., Tan, Z., Lu, K., Yang, X., Chen, X., Wang, H., Chen, S., Fang, X., Li, S., Li, X., Liu, J., Liu, Y., Lou, S., Qiu, W., and Wang, H.: OH and HO 2 radical chemistry at a suburban site during the EXPLORE-YRD campaign in 2018, Atmos Chem Phys, 22, 7005–7028, https://doi.org/10.5194/acp-22-7005-2022, 2022.

Mao, J., Ren, X., Brune, W. H., Olson, J. R., Crawford, J. H., Fried, a., Huey, L. G., Cohen, R. C., Heikes, B., Singh, H. B., Blake, D. R., Sachse, G. W., Diskin, G. S., Hall, S. R., and Shetter, R. E.: Airborne measurement of OH reactivity during INTEX-B, Atmos Chem Phys, 9, 163–173, https://doi.org/10.5194/acp-9-163-2009, 2009.

McDonald, B. C., de Gouw, J. A., Gilman, J. B., Jathar, S. H., Akherati, A., Cappa, C. D., Jimenez, J. L., Lee-Taylor, J., Hayes, P. L., McKeen, S. A., Cui, Y. Y., Kim, S.-W., Gentner, D. R., Isaacman-VanWertz, G., Goldstein, A. H., Harley, R. A., Frost, G. J., Roberts, J. M., Ryerson, T. B., and Trainer, M.: Volatile chemical products emerging as largest petrochemical source of urban organic emissions, Science, 359, 760–764, https://doi.org/10.1126/science.aaq0524, 2018.

Mellouki, A., Wallington, T. J., and Chen, J.: Atmospheric chemistry of oxygenated volatile organic compounds: Impacts on air quality and climate, Chem Rev, 115, 3984–4014, https://doi.org/10.1021/cr500549n, 2015.

Millet, D. B., Apel, E., Henze, D. K., Hill, J., Marshall, J. D., Singh, H. B., and Tessum, C. W.: Natural and Anthropogenic Ethanol Sources in North America and Potential Atmospheric Impacts of Ethanol Fuel Use, Enviromental Science & Technology, 46, 8484–8492, 2012.

Min, K.-E., Washenfelder, R. a., Dubé, W. P., Langford, a. O., Edwards, P. M., Zarzana, K. J., Stutz, J., Lu, K., Rohrer, F., Zhang, Y., and Brown, S. S.: A broadband cavity enhanced absorption spectrometer for aircraft measurements of glyoxal, methylglyoxal, nitrous acid, nitrogen dioxide, and water vapor, Atmos Meas Tech, 9, 423–440, https://doi.org/10.5194/amt-9-423-2016, 2016.

Müller, M., Mikoviny, T., Feil, S., Haidacher, S., Hanel, G., Hartungen, E., Jordan, A., Märk, L., Mutschlechner, P., Schottkowsky, R., Sulzer, P., Crawford, J. H., and Wisthaler, A.: A compact PTR-ToF-MS instrument for airborne measurements of volatile organic compounds at high spatiotemporal resolution, Atmos Meas Tech, 7, 3763–3772, https://doi.org/10.5194/amt-7-3763-2014, 2014.

Nault, B. A., Campuzano-Jost, P., Day, D. A., Schroder, J. C., Anderson, B., Beyersdorf, A. J., Blake, D. R., Brune, W. H., Choi, Y., Corr, C. A., de Gouw, J. A., Dibb, J., DiGangi, J. P., Diskin, G. S., Fried, A., Huey, L. G., Kim, M. J., Knote, C. J., Lamb, K. D., Lee, T., Park, T., Pusede, S. E., Scheuer, E., Thornhill, K. L., Woo, J.-H., and Jimenez, J. L.: Secondary organic aerosol production from local emissions dominates the organic aerosol budget over Seoul, South Korea, during KORUS-AQ, Atmos Chem Phys, 18, 17769–17800, https://doi.org/10.5194/acp-18-17769-2018, 2018.

https://doi.org/10.5194/egusphere-2024-596
Preprint. Discussion started: 2 April 2024

Nihill, K. J., Ye, Q., Majluf, F., Krechmer, J. E., Canagaratna, M. R., and Kroll, J. H.: Influence of the NO/NO_2 Ratio on Oxidation Product Distributions under High-NO Conditions, Environ Sci Technol, 55, 6594–6601, https://doi.org/10.1021/acs.est.0c07621, 2021.

Orlando, J. J. and Tyndall, G. S.: Laboratory studies of organic peroxy radical chemistry: an overview with emphasis on recent issues of atmospheric significance, Chem Soc Rev, 41, 6294–6317, https://doi.org/10.1039/c2cs35166h, 2012.

Park, R. J., Oak, Y. J., Emmons, L. K., Kim, C. H., Pfister, G. G., Carmichael, G. R., Saide, P. E., Cho, S. Y., Kim, S., Woo, J. H., Crawford, J. H., Gaubert, B., Lee, H. J., Park, S. Y., Jo, Y. J., Gao, M., Tang, B., Stanier, C. O., Shin, S. S., Park, H. Y., Bae, C., and Kim, E.: Multi-model intercomparisons of air quality simulations for the KORUS-AQ campaign, Elementa, 9, 1–29, https://doi.org/10.1525/elementa.2021.00139, 2021.

Perring, A. E., Bertram, T. H., Farmer, D. K., Wooldridge, P. J., Dibb, J., Blake, N. J., Blake, D. R., Singh, H. B., Fuelberg, H., Diskin, G., Sachse, G., and Cohen, R. C.: The production and persistence of $\Sigma RONO_2$ in the Mexico City plume, Atmos Chem Phys, 10, 7215–7229, https://doi.org/10.5194/acp-10-7215-2010, 2010.

Perring, A. E., Pusede, S. E., and Cohen, R. C.: An observational perspective on the atmospheric impacts of alkyl and multifunctional nitrates on ozone and secondary organic aerosol., Chem Rev, 113, 5848–70, https://doi.org/10.1021/cr300520x, 2013.

Peterson, D. A., Hyer, E. J., Han, S. O., Crawford, J. H., Park, R. J., Holz, R., Kuehn, R. E., Eloranta, E., Knote, C., Jordan, C. E., and Lefer, B. L.: Meteorology influencing springtime air quality, pollution transport, and visibility in Korea, Elementa, 7, https://doi.org/10.1525/elementa.395, 2019.

Picquet-Varrault, B., Suarez-Bertoa, R., Duncianu, M., Cazaunau, M., Pangui, E., David, M., Doussin, J., Cnrs, U. M. R., Créteil, U. P., Paris, U. De, Pierre, I., and Laplace, S.: Photolysis and oxidation by OH radicals of two carbonyl nitrates : 4-nitrooxy-2-butanone and 5-nitrooxy-2-pentanone, Atmos Chem Phys, 20, 487–498, https://doi.org/10.5194/acp-20-487-2020, 2020.

Rao, H., Fullana, A., Sidhu, S., and Carbonell-barrachina, Á. A.: Emissions of volatile aldehydes from heated cooking oils, Food Chem, 120, 59–65, https://doi.org/10.1016/j.foodchem.2009.09.070, 2010.

Ren, X., Duin, D. Van, Cazorla, M., Chen, S., Mao, J., Zhang, L., Brune, W. H., Flynn, J. H., Grossberg, N., Lefer, B. L., Rappenglück, B., Wong, K. W., Tsai, C., Stutz, J., Dibb, J. E., Jobson, B. T., Luke, W. T., and Kelley, P.: Atmospheric oxidation chemistry and ozone production : Results from SHARP 2009 in Houston, Texas, Journal of Geophysical Research: Atmospheres, 118, 5770–5780, https://doi.org/10.1002/jgrd.50342, 2013.

Richter, D., Weibring, P., Walega, J. G., Fried, A., Spuler, S. M., and Taubman, M. S.: Compact highly sensitive multi-species airborne mid-IR spectrometer, Applied Physics B, 119, 119–131, https://doi.org/10.1007/s00340-015-6038-8, 2015.

Rosen, R. S., Wood, E. C., Wooldridge, P. J., Thornton, J. A., Day, D. A., Kuster, W., Williams, E. J., Jobson, B. T., and Cohen, R. C.: Observations of total alkyl nitrates during Texas Air Quality Study 2000 : Implications for O_3 and alkyl nitrate photochemistry, J Geophys Res, 109, D07303, https://doi.org/10.1029/2003JD004227, 2004.

https://doi.org/10.5194/egusphere-2024-596
Preprint. Discussion started: 2 April 2024

Sachse, G. W., Hill, G. F., Wade, L. O., and Perry, M. G.: Fast-Response, High-Precision Carbon Monoxide Sensor using a Tunable Diode Laser Absorption Technique, Journal of Geophysical Research: Atmospheres, 92, 2071–2081, https://doi.org/doi:10.1029/JD092iD02p02071, 1987.

Sai, S., Ho, H., Yu, J. Z., Chu, K. W., Yeung, L. L., Sai, S., Ho, H., Yu, J. Z., Chu, K. W., and Yeung, L. L.: Carbonyl Emissions from Commercial Cooking Sources in Hong Kong Carbonyl Emissions from Commercial Cooking Sources in Hong Kong, J Air Waste Manage Assoc, 56, 1091–1098, https://doi.org/10.1080/10473289.2006.10464532, 2012.

Saunders, S. M., Jenkin, M. E., Derwent, R. G., and Pilling, M. J.: Protocol for the development of the Master Chemical Mechanism, MCM v3 (Part A): tropospheric degradation of non-aromatic volatile organic compounds, Atmos Chem Phys, 3, 161–180, https://doi.org/10.5194/acp-3-161-2003, 2003.

Schauer, J. J., Kleeman, M. J., Cass, G. R., and Simoneit, B. R. T.: Measurement of Emissions from Air Organic Compounds from Cooking with Seed Oils, Environ Sci Technol, 36, 567–575, https://doi.org/10.1021/es002053m, 2002.

von Schneidemesser, E., McDonald, B. C., Denier van der Gon, H., Crippa, M., Guizzardi, D., Borbon, A., Dominutti, P., Huang, G., Jansens-Maenhout, G., Li, M., Ou-Yang, C. F., Tisinai, S., and Wang, J. L.: Comparing Urban Anthropogenic NMVOC Measurements With Representation in Emission Inventories—A Global Perspective, Journal of Geophysical Research: Atmospheres, 128, https://doi.org/10.1029/2022JD037906, 2023.

Schroeder, J. R., Crawford, J. H., Ahn, J. Y., Chang, L., Fried, A., Walega, J., Weinheimer, A., Montzka, D. D., Hall, S. R., Ullmann, K., Wisthaler, A., Mikoviny, T., Chen, G., Blake, D. R., Blake, N. J., Hughes, S. C., Meinardi, S., Diskin, G., Digangi, J. P., Choi, Y., Pusede, S. E., Huey, G. L., Tanner, D. J., Kim, M., and Wennberg, P.: Observation-based modeling of ozone chemistry in the Seoul metropolitan area during the Korea-United States Air Quality Study (KORUS-AQ), Elementa, 8, https://doi.org/10.1525/elementa.400, 2020.

Seo, J., Park, D. R., Kim, J. Y., Youn, D., Lim, Y. Bin, and Kim, Y.: Effects of meteorology and emissions on urban air quality : a quantitative statistical approach to long-term records (1999 – 2016) in Seoul , South Korea, Atmos Chem Phys, 18, 16121–16137, 2018.

Shetter, R. E. and Müller, M.: Photolysis frequency measurements using actinic flux spectroradiometry during the PEM-Tropics mission: Instrumentation description and some results, Journal of Geophysical Research-Atmospheres, 104, 5647–5661, https://doi.org/10.1029/98JD01381, 1999.

Simpson, I. J., Blake, D. R., Blake, N. J., Meinardi, S., Barletta, B., Hughes, S. C., Fleming, L. T., Crawford, J. H., Diskin, G. S., Emmons, L. K., Fried, A., Guo, H., Peterson, D. A., Wisthaler, A., Woo, J., Barré, J., Gaubert, B., Kim, J., Kim, M. J., Kim, Y., Knote, C., Mikoviny, T., Sally, E., Schroeder, J. R., Wang, Y., Wennberg, P. O., and Zeng, L.: Characterization , sources and reactivity of volatile organic compounds (VOCs) in Seoul and surrounding regions during KORUS-AQ, Elementa: Science of the Anthropocene, 8, 37, https://doi.org/10.1525/elementa.434, 2020.

Sprengnether, M. M., Demerjian, K. L., Dransfield, T. J., Clarke, J. S., Anderson, J. G., and Donahue, N. M.: Rate Constants of Nine C6-C9 Alkanes with OH from 230 to 379 K: Chemical Tracers for [OH] , J Phys Chem A, 113, 5030–5038, https://doi.org/10.1021/jp810412m, 2009.

https://doi.org/10.5194/egusphere-2024-596
Preprint. Discussion started: 2 April 2024

Tan, Z., Lu, K., Hofzumahaus, A., Fuchs, H., Bohn, B., Holland, F., Liu, Y., Rohrer, F., Shao, M., Sun, K., Wu, Y., Zeng, L., Zhang, Y., Zou, Q., Kiendler-Scharr, A., Wahner, A., and Zhang, Y.: Experimental budgets of OH, HO_2, and RO_2 radicals and implications for ozone formation in the Pearl River Delta in China 2014, Atmos Chem Phys, 19, 7129–7150, https://doi.org/10.5194/acp-19-7129-2019, 2019.

Teng, A. P., Crounse, J. D., Lee, L., St Clair, J. M., Cohen, R. C., and Wennberg, P. O.: Hydroxy nitrate production in the OH-initiated oxidation of alkenes, Atmos Chem Phys, 15, 4297–4316, https://doi.org/10.5194/acp-15-4297-2015, 2015.

Thornton, J. A., Wooldridge, P. J., and Cohen, R. C.: Atmospheric NO_2: In-situ laser-induced fluorescence detection at parts per trillion mixing ratios, Anal Chem, 72, 528–539, https://doi.org/doi:10.1021/ac9908905, 2000.

Travis, K. R., Crawford, J. H., Chen, G., Jordan, C. E., Nault, B. A., Kim, H., Jimenez, J. L., Campuzano-Jost, P., Dibb, J. E., Woo, J. H., Kim, Y., Zhai, S., Wang, X., McDuffie, E. E., Luo, G., Yu, F., Kim, S., Simpson, I. J., Blake, D. R., Chang, L., and Kim, M. J.: Limitations in representation of physical processes prevent successful simulation of PM2.5 during KORUS-AQ, Atmos Chem Phys, 22, 7933–7958, https://doi.org/10.5194/acp-22-7933-2022, 2022.

Tuite, K., Thomas, J. L., Veres, P. R., and Roberts, J. M.: Quantifying Nitrous Acid Formation Mechanisms Using Measured Vertical Profiles During the CalNex 2010 Campaign and 1D Column Modeling, Journal of Geophysical Research: Atmospheres, 126, e2021JD034689, https://doi.org/10.1029/2021JD034689, 2021.

Wang, W., Yuan, B., Peng, Y., Su, H., Cheng, Y., Yang, S., Wu, C., Qi, J., Bao, F., Huangfu, Y., Wang, C., Ye, C., Wang, Z., Wang, B., Wang, X., Song, W., Hu, W., Cheng, P., Zhu, M., Zheng, J., and Shao, M.: Direct observations indicate photodegradable oxygenated volatile organic compounds (OVOCs) as larger contributors to radicals and ozone production in the atmosphere, Atmos Chem Phys, 22, 4117–4128, https://doi.org/10.5194/acp-22-4117-2022, 2022.

Wargocki, P., Weschler, J., and Williams, J.: Assessment of aldehyde contributions to PTR-MS m/z 69.07 in indoor air measurements, Environmental Science: Atmospheres, Advance Ar, https://doi.org/10.1039/d3ea00055a, 2023.

Weinheimer, A. J., Walega, J. G., Ridley, B. A., Gary, B. L., Blake, D. R., Blake, N. J., Rowland, F. S., Sachse, G. W., Anderson, B. E., and Collins, J. E.: Meridional distributions of NO_x , NO_y , and other species in the lower stratosphere and upper troposphere during AASE II, Geophys Res Lett, 21, 2583–2586, https://doi.org/10.1029/94GL01897, 1994.

Whalley, L. K., Stone, D., Bandy, B., Dunmore, R., Hamilton, J. F., Hopkins, J., Lee, J. D., Lewis, A. C., and Heard, D. E.: Atmospheric OH reactivity in central London: observations, model predictions and estimates of in situ ozone production, Atmos Chem Phys, 16, 2109–2122, https://doi.org/10.5194/acp-16-2109-2016, 2016.

Whalley, L. K., Stone, D., Dunmore, R., Hamilton, J., Hopkins, J. R., Lee, J. D., Lewis, A. C., Williams, P., Kleffmann, J., Laufs, S., and Woodward-massey, R.: Understanding in situ ozone production in the summertime through radical observations and modelling studies during the Clean air for London project (ClearfLo), Atmos Chem Phys, 18, 2547–2571, https://doi.org/10.5194/acp-18-2547-2018, 2018.

https://doi.org/10.5194/egusphere-2024-596
Preprint. Discussion started: 2 April 2024

Whalley, L. K., Slater, E. J., Woodward-massey, R., Ye, C., Lee, J. D., Squires, F., Mehra, A., Worrall, S. D., Bacak, A., Bannan, T. J., Coe, H., and Percival, C. J.: Evaluating the sensitivity of radical chemistry and ozone formation to ambient VOCs and NO_x in Beijing, Atmos Chem Phys, 21, 2125–2147, https://doi.org/10.5194/acp-21-2125-2021, 2021.

Wolfe, G. M., Marvin, M. R., Roberts, S. J., Travis, K. R., and Liao, J.: The Framework for 0-D Atmospheric Modeling (F0AM) v3.1, Geosci Model Dev, 9, 3309–3319, https://doi.org/10.5194/gmd-9-3309-2016, 2016.

Wooldridge, P. J., Perring, A. E., Bertram, T. H., Flocke, F. M., Roberts, J. M., Singh, H. B., Huey, L. G., Thornton, J. A., Wolfe, G. M., Murphy, J. G., Fry, J. L., Rollins, A. W., LaFranchi, B. W., and Cohen, R. C.: Total Peroxy Nitrates (ΣPNs) in the atmosphere: the Thermal Dissociation-Laser Induced Fluorescence (TD-LIF) technique and comparisons to speciated PAN measurements, Atmos Meas Tech, 3, 593–607, https://doi.org/DOI 10.5194/amt-3-593-2010, 2010.

Xu, Y., Feng, X., Chen, Y., Zheng, P., Hui, L., Chen, Y., Yu, J. Z., and Wang, Z.: Development of an enhanced method for atmospheric carbonyls and characterizing their roles in photochemistry in subtropical Hong Kong, Science of The Total Environment, 896, 165135, https://doi.org/10.1016/j.scitotenv.2023.165135, 2023.

Yang, G., Huo, J., Wang, L., Wang, Y., Wu, S., Yao, L., Fu, Q., and Wang, L.: Total OH Reactivity Measurements in a Suburban Site of Shanghai J, Journal of Geophysical Research: Atmospheres, 127, 1–20, https://doi.org/10.1029/2021JD035981, 2022.

Yeh, G. K. and Ziemann, P. J.: Alkyl nitrate formation from reactions of C8-C14 n-alkanes with OH radicals in the presence of NOx: Measured yields with essential corrections for gas-wall partitioning, Journal of Physical Chemistry A, 118, 8147–8157, https://doi.org/10.1021/jp500631v, 2014.

Yeo, M. J. and Kim, Y. P.: Long-term trends of surface ozone in Korea, J Clean Prod, 294, 125352, https://doi.org/10.1016/j.jclepro.2020.125352, 2021.

Yuan, B., Shao, M., de Gouw, J., Parrish, D. D., Lu, S., Wang, M., Zeng, L., Zhang, Q., Song, Y., Zhang, J., and Hu, M.: Volatile organic compounds (VOCs) in urban air: How chemistry affects the interpretation of positive matrix factorization (PMF) analysis, Journal of Geophysical Research: Atmospheres, 117, n/a-n/a, https://doi.org/10.1029/2012JD018236, 2012.

Zare, A., Romer, P. S., Nguyen, T., Keutsch, F. N., Skog, K., and Cohen, R. C.: A comprehensive organic nitrate chemistry: Insights into the lifetime of atmospheric organic nitrates, Atmos Chem Phys, 18, 15419–15436, https://doi.org/10.5194/acp-18-15419-2018, 2018.

Zhao, Y., Hennigan, C. J., May, A. A., Tkacik, D. S., De Gouw, J. A., Gilman, J. B., Kuster, W. C., Borbon, A., and Robinson, A. L.: Intermediate-volatility organic compounds: A large source of secondary organic aerosol, Environ Sci Technol, 48, 13743–13750, https://doi.org/10.1021/es5035188, 2014.

Zhou, Z., Tan, Q., Deng, Y., Song, D., Wu, K., Zhou, X., Huang, F., Zeng, W., and Lu, C.: Compilation of emission inventory and source profile database for volatile organic compounds : A case study for Sichuan, China, Atmos Pollut Res, 11, 105–116, https://doi.org/10.1016/j.apr.2019.09.020, 2020.

https://doi.org/10.5194/egusphere-2024-596
Preprint. Discussion started: 2 April 2024

Tables

Table 1. Reactions described in text along with associated rate constants and references for those rate constants.

	Reaction	*Reaction Rate*	*Reference*
R1a	$VOC+OH \xrightarrow{O_2} RO_2^{\cdot}$	Varies	Atkinson (2003); Atkinson and Arey(2003); Atkinson et al. (2006); Bohn and Zetzsch (2012); Sprengnether et al. (2009)
R1b	$VOC+h\nu \xrightarrow{O_2} RO_2^{\cdot}$	Varies/Measured	Shetter & Müller (1999)
R2a	$RO_2^{\cdot}+NO \rightarrow (1-\alpha)\ RO^{\cdot}+(1-\alpha)\ NO_2$	$2.7\times10^{-11}\times\exp(390/T)$	Burkholder et al. (2020)
R2b	$RO_2^{\cdot}+NO \rightarrow \alpha\ RONO_2$	$2.7\times10^{-11}\times\exp(390/T)$	Burkholder et al. (2020)
R3	$NO_2+h\nu \rightarrow NO+O(^3P)$	Measured on DC-8	Shetter & Müller (1999)
R4	$O(^3P)+O_2 \rightarrow O_3$	$3.2\times10^{-11}\times\exp(67/T)$	Saunders et al. (2003)
R5	$RO^{\cdot}+O_2 \rightarrow R(O)+HO_2$	Assumed Instantaneous	
R6	$HO_2+NO \rightarrow OH+NO_2$	$3.45\times10^{-12}\times\exp(270/T)$	Saunders et al. (2003)
R7	$RCHO+OH \xrightarrow{O_2} R(O)O_2^{\cdot}$	Varies	Atkinson (2003); Atkinson and Arey(2003); Atkinson et al. (2006)
R8[a]	$R(O)O_2^{\cdot}+NO_2 \leftrightarrow R(O)O_2NO_2$	F: 8.69×10^{-12} cm^3 molec.$^{-1}$ s^{-1} R: 4.30×10^{-4} s^{-1}	Burkholder et al. (2020)
R9	$R(O)O_2+NO \rightarrow RO_2^{\cdot}+NO_2$	$8.1\times10^{-12}\times\exp(270/T)$	Burkholder et al. (2020)
R10	$O_3+NO \rightarrow O_2+NO_2$	$2.07\times10^{-12}\times(-1400/T)$	Burkholder et al. (2020)
R11[b]	$OH+NO_2 \rightarrow HNO_3$	1.24×10^{-11} cm^3 molec.$^{-1}$ s^{-1}	Burkholder et al. (2020)
R12	$O_3+h\nu \xrightarrow{H_2O} 2O(^1D)$	hν measured on DC-8; 2.14×10^{-10} cm^3 molec.$^{-1}$ s^{-1}	Shetter & Müller (1999); Saunders et al. (2003)
R13	$O_3+OH \rightarrow HO_2+O_2$	$1.7\times10^{-12}\times\exp(-940/T)$	Saunders et al. (2003)
R14	$O_3+HO_2 \rightarrow OH+2O_2$	$1.0\times10^{-14}\times\exp(-490/T)$	Burkholder et al. (2020)
R15[b]	$HO_2+HO_2 \xrightarrow{H_2O} H_2O_2$	5.06×10^{-12} cm^3 molec.$^{-1}$ s^{-1}	Saunders et al. (2003)
R16	$HO_2+RO_2 \rightarrow$ Products	$2.91\times10^{-13}\times\exp(1300/T)$	Saunders et al. (2003)
R17	$HO_2+0H \rightarrow$ Products	$4.80\times10^{-11}\times\exp(250/T)$	Burkholder et al. (2020)

https://doi.org/10.5194/egusphere-2024-596
Preprint. Discussion started: 2 April 2024

R18[b]	OH+NO → HONO	7.40×10^{-12} cm^3 $molec.^{-1}$ s^{-1}	Burkholder et al. (2020)
R19	HO_2+R(O)O_2 → Products	$4.30\times10^{-13}\times\exp(1040/T)$	Burkholder et al. (2020)

[a]Only showing forward (F) and reverse (R) rate constant at 298 K and 1013 hPa and being a termolecular reaction.
[b]Termolecular reaction; only showing rate at 298 K and 1013 hPa

https://doi.org/10.5194/egusphere-2024-596
Preprint. Discussion started: 2 April 2024

Table 2. List of instruments, compounds measured, accuracy/precision, and associated references used in this study.

Instrument	Species	References
University of California, Irvine, Whole Air Sampler (WAS)	Ethane, Ethene, Ethyne, Propane, Propene, i-Butane, n-Butane, 1-Butene, i-Butene, trans-2-Butene, cis-2-Butene i-Pentane, n-Pentane, 1,3-Butadiene, Isoprene, n-Hexane, n-Heptane, n-Octane, n-Nonane, n-Decane, 2,3-Dimethylbutane, 2-Methylpentane, 3-Methylpentane, Cyclopentane, Methylcyclopentane, Cyclohexane, Methylcyclohexane, Benzene, Toluene, m+p-Xylene, o-Xylene, Ethylbenzene, Styrene, i-Propylbenzene, n-Propylbenzene, 3-Ethyltoluene, 4-Ethyltoluene, 2-Ethyltoluene, 1,3,5-Trimethylbenzene, 1,2,4-Trimethylbenzene, 1,2,3-Trimethylbenzene, α-Pinene, β-Pinene, Methyl nitrate, Ethyl nitrate, i-Propyl nitrate, n-Propyl nitrate, 2-Butyl nitrate, 3-Pentyl nitrate, 2-Pentyl nitrate, 3-Methyl-2-Butyl nitrate	Simpson et al. (2020)
The Pennsylvania State University Airborne Tropospheric Hydrogen Oxides Sensor (ATHOS)	OH, HO_2, OH Reactivity	Faloona et al. (2004), Mao et al. (2009), Brune et al. (2019)
University of California, Berkeley, Thermal Dissociation-Laser Induced Fluorescence (TD-LIF)	NO_2, ΣPNs, ΣANs	Thornton et al. (2000), Day et al. (2002), Wooldridge et al. (2010)
NASA Langley Diode Laser Hygrometer (DLH)	H_2O	Diskin et al. (2002)
NASA Langley Diode Laser Spectrometer Measurements (DACOM)	CO, CH_4	Sachse et al. (1987)
University of Colorado, Boulder, Compact Atmospheric Multi-species Spectrometer (CAMS)	CH_2O, C_2H_6	Richter et al. (2015), Fried et al. (2020)
Gwangju Institute of Science and Technology Korean Airborne Cavity Enhances Spectrometer (K-ACES)	CHOCHO	Min et al. (2016), D. Kim et al. (2022)

https://doi.org/10.5194/egusphere-2024-596
Preprint. Discussion started: 2 April 2024

NCAR CCD Actinic Flux Spectroradiometers (CAFS)	j-values	Shetter & Müller (1999)
Georgia Institute of Technology Chemical Ionization Mass Spectrometer (GT)	SO_2, PAN, PPN, APAN, PBzN	Kim et al. (2007), Lee et al. (2022)
University of Colorado, Boulder, High-Resolution Time-of-Flight Aerosol Mass Spectrometer	pNO_3	Nault et al. (2018), Day et al. (2022)
NCAR 4-Channel Chemiluminescence Instrument (NCAR)	NO, NO_2, O_3, NO_y	Weinheimer et al. (1994)
California Institute of Technology Chemical Ionization Mass Spectrometer (CIT)	Butene Hydroxynitrates, Butadiene Hydroxnitrates, Ethene Hydroxynitrates, Ethanal Nitrate, Isoprene Hydroxynitrates, Propene Hydroxynitrates, Propanal Nitrate, CH_3OOH, Peroxyacetic Acid, HNO_3, Hydroxyacetone, H_2O_2	Crounse et al. (2006), Teng et al. (2015)
University of Oslo Proton Transfer Reaction Time-of-Flight Mass Spectrometer (PTR-MS)	Methanol, Acetaldehyde, Acetone+Propanal, Isoprene, MVK+MACR+ISOPOOH, Benzene, Toluene, C8-alkylbenzenes, Monoterpenes, MEK	Müller et al. (2014)
NSRC Meteorological and Geographical Data	Latitude, Longitude, Altitude, Temperature, Pressure	Crawford et al. (2021)

1191

https://doi.org/10.5194/egusphere-2024-596
Preprint. Discussion started: 2 April 2024

1192 **Figures**

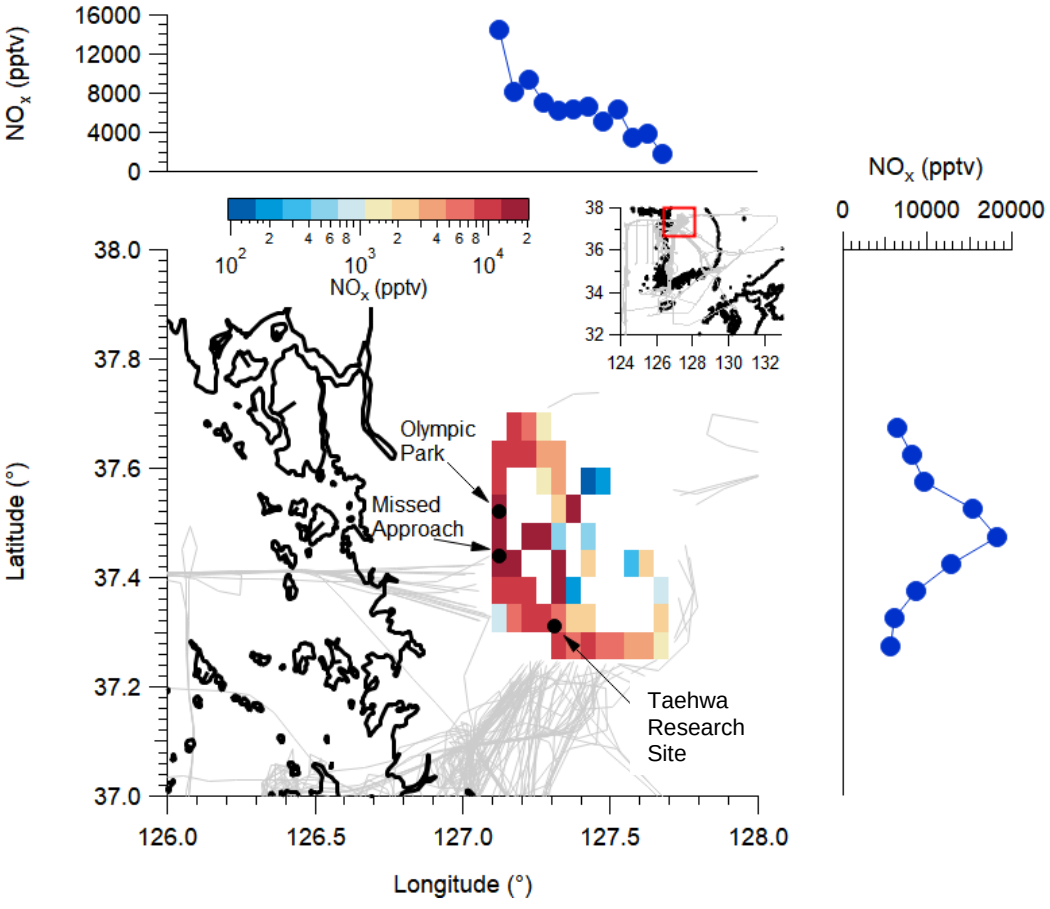

1193

1194 **Figure 1.** Binned NO_x mixing ratios observed on the NASA DC-8 during the KORUS-AQ
1195 campaign. Note, the color bar scale is logarithmic. The binning is along the flight paths of the
1196 NASA DC-8 for any observations collected below 2.0 km and after 11:00 local time. The rest of
1197 the NASA DC-8 flight paths not included in the analysis are shown in grey. Three key areas from
1198 KORUS-AQ are highlighted—the Olympic Park ground site, the airfield where the NASA DC-8
1199 conducted routine missed approaches, and the Taehwa Research ground site. The histograms
1200 above and to the left are the distribution of NO_x mixing ratios longitudinally and latitudinally,
1201 respectively.

https://doi.org/10.5194/egusphere-2024-596
Preprint. Discussion started: 2 April 2024

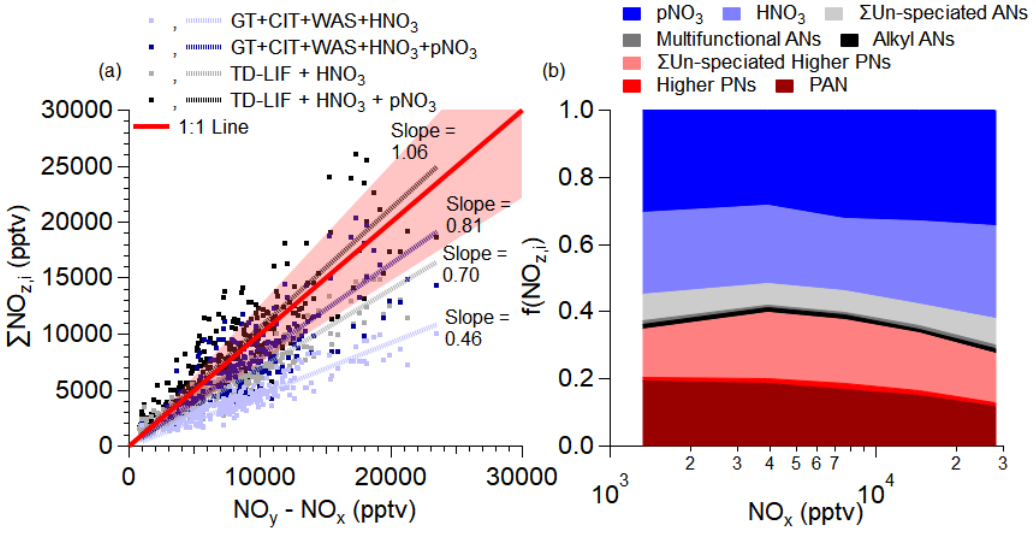

1202

1203 **Figure 2.** (a) Scatter plot of the summation of individual NO_z (NO_z is higher oxide NO_x products)
1204 measured by GT, CIT, WAS, TD-LIF, and AMS versus NO_z measured by difference between NO_y
1205 and NO_x (see Table 2 for compounds measured by each instrument). NO_x is NO measured by
1206 NCAR and NO_2 measured by LIF. The observations are for when the DC-8 was over the SMA.
1207 (b) Average contribution of measured speciated NO_z over the SMA during KORUS-AQ versus
1208 NO_x. Higher PNs is PPN + APAN + PBZN. ΣUn-speciated PNs is total peroxnitrates from TD-
1209 LIF minus total measurement from GT. Alkyl $RONO_2$ is the total small alkyl nitrate measurements
1210 from WAS. Multifunctional $RONO_2$ is the total measurements from CIT. ΣUn-speciated ANs is
1211 the total alkyl nitrates from TD-LIF minus total $RONO_2$ from CIT and WAS.

https://doi.org/10.5194/egusphere-2024-596
Preprint. Discussion started: 2 April 2024

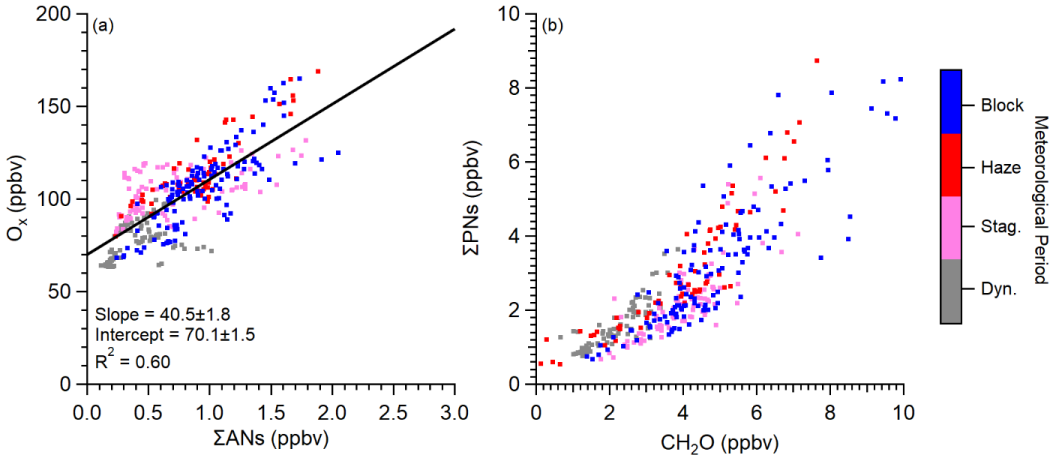

Figure 3. Scatter plot of (a) O_x versus ΣANs and (c) ΣPNs versus formaldehyde (CH_2O) over SMA (see Figure 1 for area studied). Data is colored by meteorological periods discussed in Peterson et al. (2019). Data plotted here is after 11:00 am LT to minimize impact of growing boundary layer and nocturnal residual layer mixing. The curvature in (c) is further explored in Figure S7.

https://doi.org/10.5194/egusphere-2024-596
Preprint. Discussion started: 2 April 2024

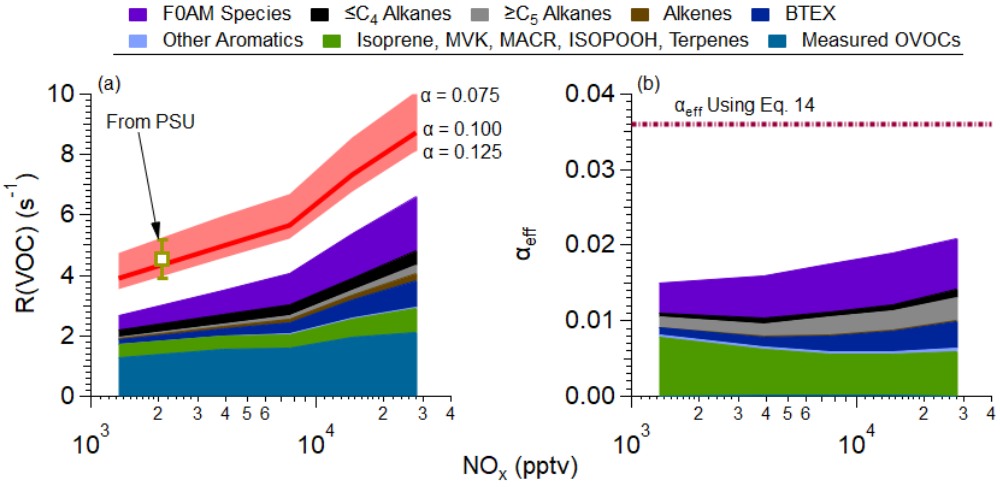

Figure 4. (a) Binned VOC reactivity versus NO_x observed over SMA during KORUS-AQ (see Figure 1 for the area studied). The measured observed R(VOC), labeled as "From PSU", where PSU is Pennsylvania State University, is the VOC reactivity calculated from the measured total OH reactivity with inorganic OH reactivity removed. As discussed in Brune et al. (2022), the OH reactivity has interferences at high NO_x mixing ratios. The error bar is the uncertainty in the OH reactivity measurement (Brune et al., 2022). The red line represents the calculated unmeasured R(VOC), using Eq. 11, with an assumed $\alpha = 0.10$. The shaded area represents different calculated unmeasured R(VOC), assuming different α for the unmeasured R(VOC) (see Eq. 11). (b) The calculated effective α from observations versus NO_x. The dashed purple line is the effective α estimated from Eq. 10, using the slope from Figure 3a. For both (a) and (b), the colored stacked data is the calculated VOC reactivity (a) and weighted effective α (b). The values from (b) are calculated using Eq. 11. Finally, for both (a) and (b), F0AM species is the reactivity for compounds not measured on the DC-8 predicted by F0AM with an estimated $\alpha = 0.05$. The associated uncertainty in using different α for the F0AM predicted reactivity is explored in Figure S4.

https://doi.org/10.5194/egusphere-2024-596
Preprint. Discussion started: 2 April 2024

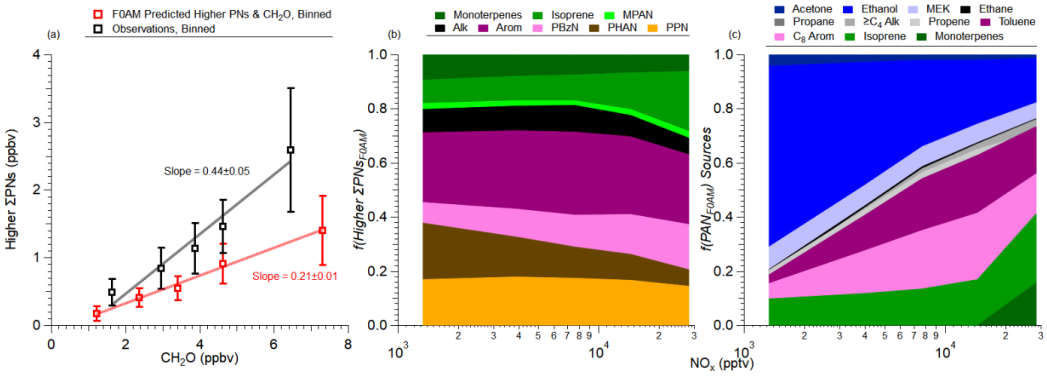

Figure 5. (a) Scatter plot of binned higher ΣPNs calculated using F0AM (red) or binned higher ΣPNs from observations (black) versus formaldehyde (CH_2O). Slopes shown are ODR fits to the binned data. (b) Fractional contribution of the higher PNs predicted from F0AM versus NO_x. (c) Fractional contribution of different precursors to PAN, predicted by F0AM versus NO_x. For both (b) and (c), Alk is all alkanes, Arom is all aromatics, and ≥C_4 Alk is all alkanes with 4 or more carbons. See Figure S8 for comparison of F0AM.

https://doi.org/10.5194/egusphere-2024-596
Preprint. Discussion started: 2 April 2024

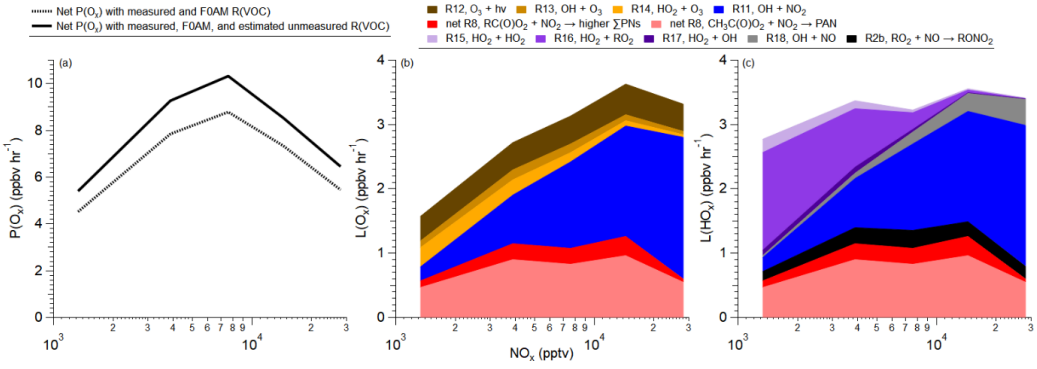

1240

1241 **Figure 6.** (a) Net O_x (O_3 + NO_2) production (see Eq. 1 and 2) predicted for SMA using measured
1242 and F0AM R(VOC) (dashed) or total R(VOC) (solid), from Figure 4a, versus NO_x. (b)
1243 Contribution of different reactions to the total O_x loss versus NO_x. (c) Contribution of different
1244 reactions to total HO_x (HO_x = OH + HO_2 + RO_2 + $R(O)O_2$) loss versus NO_x. The predicted RO_2
1245 comes from the total VOC reactivity calculated in Figure 4a assuming steady-state (Eq. 7), and
1246 HO_2 the acyl peroxy radicals are from F0AM results. Note for both (b) and (c), net $RC(O)O_2$ +
1247 NO_2 and net $CH_3C(O)O_2$ + NO_2 are described in Eq. 3. Radical reactions contributing < 1% to the
1248 $L(O_x)$ or $L(HO_x)$ are not included.

https://doi.org/10.5194/egusphere-2024-596
Preprint. Discussion started: 2 April 2024

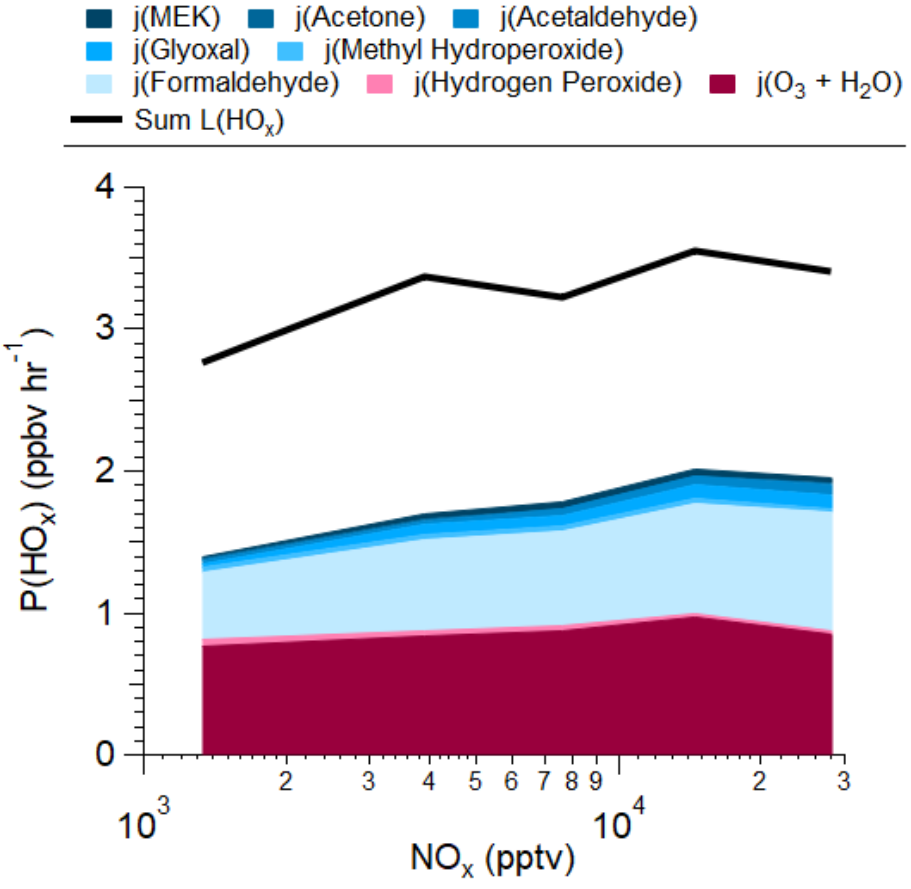

Figure 7. Calculated HO_x production from observations (colored stack) compared with the calculated HO_x loss from Figure 6c over the SMA during KORUS-AQ.